HHS Public Access

Author manuscript

Anal Chem. Author manuscript; available in PMC 2019 March 18.

Published in final edited form as:

Anal Chem. 2018 February 06; 90(3): 1444–1463. doi:10.1021/acs.analchem.7b05330.

Infrared Spectroscopic Imaging Advances as an Analytical Technology for Biomedical Sciences

Tomasz P. Wrobel[†,‖] and **Rohit Bhargava**[*,†,§]

[†]Beckman Institute for Advanced Science and Technology, Urbana, Illinois 61801, United States

[§]Departments of Bioengineering, Electrical and Computer Engineering, Mechanical Science and Engineering, Chemical and Biomolecular Engineering, and Chemistry, University of Illinois at Urbana−Champaign, Urbana, Illinois 61801, United States

Optical chemical imaging seeks to nondestructively acquire spatially resolved chemical information without the use of labels or probes. The combination of vibrational mid-infrared (IR) spectroscopy and microscopy is especially attractive since the fundamental vibrational modes of samples are coincident with optical frequencies, thereby absorbing a large fraction of incident light and providing a strong signal. Modern IR spectroscopic imaging can be traced back nearly 25 years, with the coupling of an IR microscope to an array detector and an interferometer. [1,2] Instrumentation had been largely similar to this initial setup for almost two decades with several innovations such as rapid scan imaging, [3,4] time-resolved imaging, [5] faster detectors, and linear array systems.[6] These advances have provided several variants to speed up data acquisition and enable new capabilities compared to the basic configuration of a broadband globar source, interferometer, and array detector-equipped microscope. Recent advances in hardware and design have dramatically changed both instrumentation and availability over the past few years. The availability of new components has led to a diversity in instrumentation; new understanding of image formation by rigorous theory has led to new designs and, consequently, novel applications have resulted in notable progress. A tremendous expansion in capability and exciting new possibilities for analytical measurements have now become apparent. Here, we review these advances and organize the various developments in the framework of transforming the analytical performance of IR imaging in terms of spatial, temporal, and information content.

Several excellent reviews cover the fundamentals of the technology, [7] instrumentation,[8,9] and applications[9–11] as well as applications in polymers, [12,13] plant biology,[14] pharmaceuticals, explosives, forensic applications, [15] and aspects of biomedical imaging. [16–18] In terms of instrumentation, most reviews naturally focus on Fourier transform IR (FT-IR) imaging technology using array detectors. Briefly, a state-of-the-art FT-IR imaging system consists of a microscope (Figure 1) with a focal plane array (FPA) detector. The most common detector material is mercury−cadmium−telluride (MCT) to enable wide sensitivity

[*]Corresponding Author rxb@illinois.edu.

[‖]Present Address T.P.W.: Institute of Nuclear Physics, Polish Academy of Sciences, Krakow, Poland, PL-31342.

Notes

The authors declare no competing financial interest.

in the mid-IR, and the sensing element is liquid nitrogen cooled to ensure high signal-to-noise ratios (SNR). IR microscopes in this format are coupled to a Michelson interferometer-based spectrometer equipped with a broadband thermal source (Globar). While the source and interferometer have been relatively similar across all major manufacturers, detectors may be linear or two-dimensional arrays. The detector dimensions and image formation optics combine to provide pixel sizes that range from submicrometer to tens of micrometers in different optical configurations. A globar source is commonly used in benchtop systems to obtain a large, incoherent, broadband IR flux. Synchrotron sources are available in specialized facilities, providing much higher light flux and potentially offering superior analytical capability.[13,19] The key analytical consideration is one of obtaining the spatial detail and SNR needed to address the application need. An example for biomedical studies is shown in Figure 1. Here, the goal is to provide a chemical determination of tissue structure and disease. In current biomedical research and most tissue-level clinical diagnoses, morphologic recognition of tissue structure and disease is performed on an optical microscopy image of the sample stained with contrast agents. For example, Figure 1a shows prostate tissue stained with hematoxylin and eosin (H&E) dye. Here, nuclei (stained blue) provide the ability to find epithelial cells in patterns within the largely pink-staining stroma. In contrast, IR imaging of unstained samples does not require any dyes and the inherent chemistry of tissues provides an avenue for native contrast. A “three dimensional” data set (Figure 1c) is obtained after IR imaging, in which the two spatial dimensions provide a similar image to optical microscopy, but each pixel now contains an absorption spectrum (Figure 1d). Individual frequencies can be used from the spectrum to plot the spatial distribution of absorbance (or concentration) of individual molecular species (Figure 1e). Since many visualizations are possible from the individual components of a spectrum, computer algorithms are commonly used to convert the spectral information into application-specific knowledge. The color coded information (Figure 1f) here shows the determination of different cell types from the data. Compared to optical microscopy in which “as-recorded” data provides information for human interpretation, the spectral information content of IR imaging requires computer processing that provides information content for decision-making. A major analytical challenge lies in confidently extracting correct visualizations with a desired accuracy and often under time constraints.

The main analytical consideration in spectroscopic techniques is the SNR of the acquired data. The analytical frontiers of this technology, however, not only lie in the spectral SNR[20] but also significantly involve the spatial domain. High spatial detail affects spectral SNR, since light is now spread spatially and many more measurements are required by the detector, but high spatial detail might enhance analytical sensitivity with smaller pixels. Similarly, spectral detail involves a trade-off between higher information content and quality of data. Measurement time affects both spectral and spatial quality as well as coverage along the three-dimensional space in Figure 1c. Thus, it is very important to realize that the analytical performance of IR imaging is multidimensional and improving or relaxing constraints on one parameter strongly affects other parameters. Hence, we have organized this Review around the frontiers of analytical capability focused on recent advances in each of these major themes: spatial specificity, temporal resolution, and analytical fidelity. We first describe progress in instrumentation as a prelude to discussing each technological

aspect. Finally, we describe applications that provide significantly improved capability or take advantage of these recent advances.

ADVANCES IN PERFORMANCE VIA INSTRUMENTATION, COMPONENTS, AND OPTICAL DESIGNS

Instrumentation available today is dramatically different from just three years ago. A large part of this change is attributable to availability of new components. Increasing use of high intensity sources, i.e., the conventional synchrotron and the more recent, commercially available quantum cascade laser (QCL), has transformed the speed of data acquisition and sample preparation requirements. There are attendant benefits to using these sources, for example, in being able to use cheaper, larger-format uncooled array detectors or to provide faster/high SNR imaging by utilizing the higher signal. The new components also allow for developments in new theory that have inspired new optical designs for IR microscopes, new lenses, and control algorithms. Together, these advances are now manifested in a variety of imaging configurations that allow a diversity of recorded data and new considerations on the resolution, magnification, and quality of data. We discuss next each of these in detail.

Sources.

Quantum Cascade Lasers (QCL).—The wide bandwidth of IR spectra and lack of materials that allow lasers to be built over many frequencies had remained a challenge in realizing laser systems for mid-IR spectroscopy. Other than using single frequency lasers that are not especially useful for spectroscopy, earlier attempts focused on the development of tunable OPOs.[21] More recently, ultrabroadband and comb techniques have been developed.[22–25] Each of the techniques, however, results in expensive devices that often require careful tuning or maintenance by qualified personnel. Quantum cascade lasers (QCL)[26] are a major advance in that they are relatively easy to fabricate, are very robust and, when packaged appropriately to account for stable currents and heat management, can provide a ready-to-use component for IR imaging. A QCL does not use bulk semiconductor materials in its optically active region, thereby obviating the search for appropriate materials. QCLs consist instead of a periodic series of thin layers of varying material composition to form a superlattice. Along the length of the device, a varying electric potential is introduced by this structure. This structure is referred to as one-dimensional multiple quantum well confinement. It allows for the splitting of the band of permitted energies into a number of discrete electronic sub-bands. By engineering the layer thicknesses, a population inversion between two sub-bands can be induced to achieve laser emission. The position of the energy levels is primarily determined by the layer thicknesses; hence, the emission wavelength of QCLs can cover a wide range in the same material system and can also be tuned. An integrated single device may provide tunability over hundreds of cm^{-1}, a range that continues to increase.[27] Most commercially available systems today consist of multiple modules, with each tunable over approximately a 200−400 cm^{-1} range, to cover the full fingerprint region[28–32] using an external cavity[33,34] and grating to select frequencies.

The single frequency emission from the laser allows a discrete frequency (DF) approach to IR imaging, without a requirement for any interferometer, or additional filters. The capability to tune to a specific frequency allows any order of selection of narrow bandwidths across the spectrum. The first coupling of a QCL with an IR microscope to perform DFIR imaging was reported just in 2012 with wide field, point detection as well as the use of uncooled detectors.[28] The high output power and limited frequency measurements provide an ~100−1000-fold speed increase compared to FT-IR imaging systems.[35–38] While the limited frequency measurements provide a problem-based speedup which must be tempered by SNR considerations, the high output intensity enables sufficient illumination over a wide field of view to use room temperature bolometer detectors[9,28,39–41] that were not feasible with FT-IR imaging.[42] Additionally, QCL sources are polarized due to the nature of laser emission, allowing facile polarization studies.[31] The challenges involved in using these sources arise from the relatively high shot noise that cannot easily be mitigated by conventional measurement schemes (e.g., signal averaging), coherence effects that are apparent as speckles in images, and the still relatively high price compared to interferometers. Many of these coherent effects are lowered when a single point detector is used, and the spatial SNR of such systems is comparable to an FT-IR system.[31] While many QCL applications for gas or liquid sensing[43–49] are now available with these noise characteristics, imaging is much more difficult for a given noise level since the signal is spread over a large number of pixel detectors and cannot be fully utilized. Hence, each detector only receives a small fraction of the signal. Most importantly for spectral analysis, the wavelength range available today is limited to longer than ~4 μm, thus precluding the measurement of the important NH, OH, and CH stretching vibrational modes. QCL-based microscopes offer a practical DFIR approach and, even for continuous spectra, they offer an attractive option for IR imaging that will only become more popular in the future. Both wide field and point scanning microscopes have become commercially available. From an analytical standpoint, a greater power output and increased temporal stability of the lasers are two key directions. A third direction is to obtain stable handoff from one laser to the next in a multichip system such that the transition points are not appreciably higher in noise. In summary, however, QCLs are already reliable and being increasingly used over the past few years. This useful new source will likely drive new applications, new instrument configurations, and significant activity in IR imaging.

Synchrotrons.—The first coupling of an IR microscope to a storage ring was achieved in the 1990s;[50] since then, synchrotron facilities have been the ultimate bright and stable light sources for IR microscopy. The small size of the beam is perfectly matched to the microscopic pixel or aperture sizes used previously. For IR imaging,[50] spreading light over a large detector still provides illumination and multibeam schemes can provide exceptional performance. Their high output power has only recently been matched by QCLs, but their broadband spectral range still maintains their unparalleled position in IR imaging.[51] Approximate power output in Watts per 2 cm^{-1} bandwidth is in the range of 10^{-11}–10^{-12} for globar, 10^{-10}–10^{-11} for synchrotrons, and 10^{-6}–10^{-7} for QCL sources.[51] There are several reviews on instrument design[52–54] and applications available.[13,55,56] The recent trends in using synchrotrons have been to demonstrate ground-breaking studies and inspire laboratory translation. The high light flux, in particular, first allowed for live cell imaging in aqueous

solutions,[57–60] and similarly, initial work in IR microfluidics imaging[61–63] was performed in synchrotron facilities. Synchrotron-based microscopes served as a proof of concept work-station for first high definition IR application[64] and 3D tomography[65] as well. IR beamlines are typically one of the least expensive end stations in synchrotron facilities, and they are become more widespread with more than 25 installations currently available.[13] The necessarily limited access to these national resources and the complexity of such facilities are the main limitations of this approach for a typical user. The high quality of existing beamlines and new configurations that are expected to be online[66–71] bodes well for practitioners interested in IR imaging. These installations are likely to continue to be a user resource that allows experiments otherwise not possible in laboratories. Together with excellent, stable staff dedicated to IR imaging and a worldwide user base, impactful new science will continue to result.[72]

Filters with a Globar Source.—While higher intensities in complex sources can be obtained at some cost, as shown by examples above, surface engineering using modern lithography tools can also offer solutions. In particular, the motivation for DFIR spectroscopy and imaging led us to develop narrowband reflectance filters.[73–75] The basic technology is described in Figure 2 below. Briefly, the filters are essentially reflecting gratings whose response is engineered by careful control over dimensions and refractive indices of the materials (Figure 2). The structures themselves are easily and economically made, offering a low cost and robust alternative to spectrometers. We have also integrated the filter-source assembly into an IR microscope, showing excellent imaging capability. While more than 60 filters have been made on a single wafer, the spectral diversity is ultimately limited compared to an interferometer or a laser tunable over a broad range as individual filters have to be made. The typical full width at half-maximum is ~10 cm^{-1} for the narrowest range with these filters, which is sufficient for most condensed matter imaging. However, the weak broadband thermal source is the major issue. After loss of intensity due to the beamsplitter, relay optics, and the filter efficiency itself, wide field imaging implies that the throughput per pixel is low. With the loss of multiplexing common in FT-IR imaging using a weak source, the SNR further suffers. Hence, the technology, while interesting and potentially useful, is not especially attractive for high-fidelity imaging at present. Further development may be guided toward low cost IR devices or for specific applications (allowing no moving parts, spectrometers, for example).

Supercontinuum Sources.—There has been significant progress in supercontinuum sources with both broad bandwidths and higher intensity available.[76–79] The idea is to use a high power output pump laser in the near- or mid-infrared and couple it to an optical fiber, which by nonlinear interactions generates a broad continuum of frequencies. However, the main challenges remain, namely, in the spectral coverage, output power, and stability over such range.[80] The highest reported bandwidth values span 1−11.5 μm coverage with an average power output of ~60 mW in a limited range of 1−8 μm.[81] Up to now, these serve as point measurement fiber-optic modalities; however, evolution and incorporation into an imaging technique in the future is feasible. Closely related is the idea of upconversion, where mid-infrared frequencies are shifted by sum frequency generation[82–84] (SFG) to higher energies and fall into the range of much more sensitive near-infrared or visible

detectors. In general, nonlinear crystals used for the shift have relatively low quantum efficiency, preventing the widespread use of this approach; however, there are exceptions with the best efficiency reaching ~20%[84] and a single photon sensitivity at room temperature at a wavelength of 3 μm. The total tuning range of the device is 2.85−5 μm which also presents the second typical problem of the technique, low bandwidth. One particularly interesting use of sources has been achieved:[85] a world first coupling of a broadly tunable GaSe crystal IR source and visible laser with a photothermal induced resonance technique (PTIR) system giving a spectral coverage of 400 nm to 16 μm with a lateral resolution of up to 20 nm. This allowed one to acquire correlated vibrational and electronic properties of several materials. Frequency combs form another branch of efforts to extend the bandwidth of laser sources in the mid-infrared spectral windows.[22] They are generated by down-conversion of near-infrared, by mode-locked lasers using nonlinear crystals, or by pumping an ultrahigh quality factor microresonator with a CW laser and result in a pulse of a range of evenly spaced frequencies.[86] They offer high frequency precision (as opposed to standard QCLs), higher bandwidth, and a more stable output power, which is of critical importance in linear-infrared imaging.[22,86–88] These sources offer tremendous potential as high power, widely tunable, and tailored sources for specific wavelength regimes. Practical and robust units that realize this potential will provide the best compromise between the single frequency QCLs and the wide bandwidth thermal sources.

Lenses.

The most common type of lens for FT-IR applications is a Cassegrain objective, which is composed of two reflective mirrors, one parabolic and one hyperbolic, arranged to achieve focusing of all light wavelengths traveling through the objective. This results in minimal chromatic aberration of such a system which along with low fabrication (compared to multielement lenses) cost are the main advantages. Refractive lenses are also available and are made from mid-IR transmissive materials such as germanium.[38] Refractive lenses may provide more information content due to no need for a central obscuration and are especially useful for laser systems with their limited wavelength and ability to adjust the sample between wavelengths, both of which together will likely not cause significant chromatic aberrations. New lens designs are rapidly emerging for both reflective and refractive lenses. While the typical lens used was ~0.5 numerical aperture (NA) and had a magnification of 15×, a variety of lenses are both available and being extensively used today, ranging from 4× to 74× in magnification and 0.3 to 0.81 in NA. The effects of using a lens of specific NA and magnification not only results on spatial quality changing but also affects the spectral quality and shape. More details are provided in the theory discussion. Here, we summarize that the diversity of NA, magnification, working distances, and cost of lenses is unprecedented today and offers a rich set to design and use in individual applications. At the same time, this makes it crucial for investigators to understand the effects of using a specific lens on their recorded data and choosing components of their imaging system to optimize for the information desired. Lens design in the mid-IR has typically not been a focus for decades. New designs arising from theory and modeling of the spectral response of samples, however, have the potential to yield greater (pertinent) information. Novel designs can also provide more compact, economical systems as well as those whose performance may be tailored to

specific applications. We anticipate that there will be significantly more activity in this area in the near future.

Algorithms and Parallel Computing.

With the progressing experimental aspect of IR imaging, the data complexity and volume also increase significantly. Though computational power, storage capabilities, and other resources are expanding rapidly, the desire to survey and extract information from larger data sets has more than kept pace. In addition to hardware advances that are driven by the "big data" movement, advancements in data analysis and algorithms are also critical to scientific inquiry. In terms of data visualization of IR imaging data, a major roadblock is the requirement of creating advanced models in order to get an understanding of the obtained data. New software to model fundamental light−matter interactions is becoming available.[89] A fast algorithm for time data mining was developed,[90] and improved software packages are now available for the community (http://stim.ee.uh.edu/resources/software/siproc/). Today, an experienced user was able to separate, visualize, and evaluate the utility of the extracted tissue characteristics useful for tumor diagnosis in a few minutes, given interactive feedback. Using our older methods, simply computing a feature visualization took several minutes on a CPU. Progress has been also made in the scope of algorithms available to correct for scattering effects in the form of Extended Multiplicative Scattering Correction;[91–95] however, some of these implementations were rather expensive in terms of computational cost, and an implementation using graphical processing unit (GPU) was developed.[96,97] This area will likely remain an important focus for IR imaging and offers perhaps the greatest potential for technological progress given the rapid rate of computational hardware, algorithms, increase in data acquisition speed, and new developments in IR imaging theory. More sophisticated algorithms such as deep learning and more complex architectures of dedicated computational hardware and software that are closely integrated with instrumentation are also to be expected.

ADVANCES IN INCREASING ANALYTICAL CAPABILITY BY SPATIAL SPECIFICITY

Diffraction Limited Measurements: High Definition.

IR imaging, as any microscopic technique, is limited in the far-field spatial resolution by the diffraction limit of light unless advanced numerical processing is undertaken on additional information. Earlier optical designs approximated pixel sizes to the midband (~5 μm) point spread function; while this provides better SNR, image quality is not maximized. In order to retrieve diffraction limited spatial information, it is now becoming clear that a sufficient sampling is required, which dictates an optimal projected pixel size.[98] For full range of mid-IR (~2.5−10 μm wavelength), this pixel size is ~1 μm for high NA lenses and ~2 μm for the fingerprint region (~5−10 μm wavelength). Once this condition is met, the measurement can be termed a high definition (HD); the first experimental example was performed on the IRENI beamline in 2011.[64] This seminal study has launched a renewed interest in maximizing image quality in IR microscopy. Several major efforts were undertaken. Smaller pixels imply a lower throughput, thereby reducing SNR. The use of a synchrotron was

critical in this first demonstration since a high light throughput was required to illuminate very small, 0.54 μm pixels. Since then, thermal source HD IR imaging has been introduced and is becoming much more widespread with higher magnification objectives (up to 36×) systems.[35,99–107] Commercial systems now routinely incorporate HD optics. It must be noted that the resolution of the instrument is not the pixel size; however, optimal pixel sizes maximize image quality. The smallest pixel size and highest resolution comes from coupling of a high magnification system with a solid immersion lens that takes advantage of the high refractive index of the medium adjacent to the lens.[108,109] In this approach, with an attenuated total reflection (ATR) mode using a germanium crystal, pixel sizes of 0.25 μm × 0.25 μm[100] have been reported. To date, this remains the highest resolution and smallest pixel size reported using conventional optics and far-field detection. ATR sampling also requires the sample to be in close contact and only reports absorbance from the first ~1 μm (for Ge crystals). More practical sampling modes are transmission or transmission −reflection (transflection) in which the improvement is still substantial. Figure 3 shows an example of the gain in image quality arising from the use of HD optics. The effective pixel size in this case is approximately 30-fold smaller than that in typical conventional optics. While the image quality improvement can be appreciated, the 30-fold lower throughput would need to be compensated by signal averaging of ~900-fold times and achieving the same spectral quality by signal averaging in HD acquisitions is not feasible. In addition to synchrotrons, the emergence of broadly tunable QCLs offers a practical, high speed alternative. Given the stability and wide bandwidth of synchrotron sources, they remain the premier option. QCLs in the fingerprint region and use of signal processing strategies when using thermal sources are[110] the common options for achieving HD quality with high spectral SNR.

The benefits of HD imaging are foremost in the image quality and contrast; in the case of tissue imaging, IR imaging can resolve cellular level structures allowing one to unambiguously assign certain regions to their corresponding cell type based on histopathology. Moreover, the increased resolution reduces the volume in which a biomarker is measured facilitating its identification. All this helps in creating robust classification models, but on the down side, the scattering effects are more pronounced in HD and a question arises if those new variability sources will not prevent or diminish the capabilities of machine learning models. Recent studies on prostate[101] and breast[35] cancer tissues have shown that it is not the case and advanced classification tools can handle the increased information content. HD is very likely to become a standard in IR imaging; however, the decreased SNR puts a limit on the speed of acquisition, and new advancements in the technology are required in either broadband sources or new generation of detectors.

Imaging below the Infrared Diffraction Limit Using Visible Light: Mesoscale Imaging.

Since the detected signal imposes a limit on the spatial frequency collected in an imaging experiment, using a visible range wavelength to detect IR contrast is an excellent illustration using photothermal imaging.[111–115] In a typical embodiment, an IR source illuminates the sample, and if there is any vibrational energy levels matching with the incident frequency, IR light is absorbed causing a thermal expansion of the material as a result of relaxation. This expansion causes a refractive index change, which can be probed through the thermal

lensing mechanism using a visible laser.[116–118] The contrast, thus, is based on IR absorption, but the detected signal and spatial resolution is determined by the characteristics of visible wavelengths. An additional benefit in this scheme can be the use of high NA visible lenses, shorter wavelengths, and better detectors. More importantly, the process is a direct measure of the absorption of light (as opposed to the transmitted beam intensity that is typically measured in direct absorption spectroscopy). Given the increasing power of QCLs and easy availability of visible microscopy components, we anticipate that this mode of measurement will become more popular and commercialized shortly. The complexity of instrumentation increases; however, costs are not expected to be substantially more as the increased cost of the additional optical paths will be offset by obviating the need for expensive IR cameras. As implemented thus far, however, the approach is a point scanning one that is likely to be much slower than using multichannel detectors. A fundamental need is to lock-in to the pulsed laser, which immediately makes the technique slower compared to measuring IR intensity that can be accomplished in as little time as a single pulse. An advantage of the visible detection method may lie in the use of high powered lasers, that are more readily available, to increase SNR. Open analytical questions in this emerging modality center around describing the contrast mechanisms clearly and articulating the role of thermal diffusion and mechanical properties as well as understanding the interplay of the sample's analytical signal and contributions from neighboring media including strong absorbers such as water.

Imaging below the Diffraction Limit: Nanoscale Imaging.

Diffraction imposes a limit for minimal light spot size but does not prevent localizing a source of information below that size under certain circumstances.[119] Meeting these conditions is not possible in general, is costly in terms of measurement time and the extent of information needed, and lowers the throughput of the methods as compared to high magnification far-field approaches. One of the more straightforward approaches is to take advantage of the spatial resolution of an atomic force microscope (AFM), which is in the order of tens of nanometers, and couple the tip response with infrared light interaction with the sample. One of the more common sensing mechanisms relies on light absorption followed by a thermal expansion and relaxation of the material. The expansion magnitude is hypothesized to be proportional to IR absorbance. The influence of the mounting surface, mechanical properties, and thermal boundaries, however, has not been fully explained. The analytical sensitivity of the technique arises from high powered lasers and large expansions but can be greatly augmented by near field enhancements and locking into to high Q-factor modes of the cantilever detector. QCLs are becoming the laser of choice for such methods. The technique takes advantage of the enormous advances in the AFM field and availability of a well-validated, high-performing platform for imaging.

Another exciting approach is based on scattering,[120,121] in which the light sample interaction leads to perturbation in coherently recorded source signals. Instead of coupling an AFM, scanning near field optical microscopy (SNOM) was successfully implemented in the IR as scattering SNOM (s-SNOM).[122] An example of silk protein conformation determination is shown in Figure 4.[123] One particular implementation uses asymmetric interferometry in an elegant experiment to sensitively measure sample−tip interactions.[124]

The advantages include the use of broadband radiation and well-established interferometry for sensitive measurements by taking advantage of the Fellgett and Jacquinot advantages. The analytical challenge is to record signal from weak sources and small analytical volumes as well as the need for deconvolving algorithms; however, the technique provides access to the complete refractive index of the material in the IR, providing exquisite information. A limiting consideration is the requirement of sufficient scattering cross-section of the sample, which is rarely met in the case of biological samples, but exceptions do exist in the form of hyperspectral imaging of pure proteins or of human hair.[120] A majority of applications using this technology are in material sciences with semiconductors leading the field. Overall, the nanoscale IR imaging techniques show great promise to not only understand complex samples at an unprecedented scale but also illuminate new knowledge that is fundamental to IR measurements. Commercially named AFM-IR or nanoIR, the available technologies have seen an increasing number of applications,[125–138] mostly due to the spatial resolution below 100 nm. Progress in antenna development, tailored near fields, and enhanced modeling are expected to bring new applications as well as improved understanding of both materials and optics.

3D Imaging (Tomography, Stacking, and Depth Profiling).

The lack of 3D sectioning was a distinguishing disadvantage for IR imaging compared to conventional optical imaging as well as confocal or nonlinear Raman microscopy. One approach to addressing this need lies in measuring multiple consecutive sections[139] followed by reconstruction but has obvious time and resolution constraints while being highly cumbersome. Optical tomography is well-known in the near-infrared regime, and one implementation was reported along the lines of conventional X-ray computed tomography by taking advantage of high brilliance of a synchrotron source.[65] The projected refractive index effects (both absorption and scattering) allowed for a reconstruction of the total beam attenuation. The approach was extended from cell culture to tomographic reconstruction of a single plant cell measured with a thermal source FT-IR (Figure 5).[140] The major directions in this approach are to separate the effects of absorption from scattering so that only chemical images can be obtained as well as dealing with scattered light and condensing optics. There is another modality that offers depth profiling, ATR with variable angle of incidence, and has been implemented to macro ATR measurements previously.[141,142] Recently, it has been also extended to micro ATR measurements using a germanium crystal.[143] These measurements reflect the cumulative depth as a function of angle and need algorithms to extract specific slices at different depths. The accuracy, recovery, limits on localization, and SNR as a function of depth all remain to be established and are potential directions for analysis with this approach. Tomography techniques are expected to grow, especially with the advent of QCL sources allowing one to probe much larger samples than single cells without the use of a synchrotron. A recent review covers many of these developments in detail.[144]

Computational Enhancements to Spatial Resolution and Localization.

Whenever the point spread function (PSF) of the imaging system can be assumed to be known and properly sampled, it is possible to use deconvolution methods to increase the spatial details of already acquired images. Among methods used for deconvolution, Fourier

self deconvolution is the most commonly applied;[145–147] however, other methods such as total variation are also in use.[148] With the advent of rigorous IR microscopy theory and different methods of illumination and recording as well as the use of different substrates, one direction is likely to be the inclusion of more details of specific experiments. Another direction will likely be the use of improved computational resources for rapid deconvolution, use of specific instruments characteristic response, and real-time enhancements. Finally, deconvolution methods today do not make use of the fact that the spectral responses of a composite sample can be spectrally disjoint and can be used for finding the position of point scatterers and/or absorbers in a coherent recording experiment. Such an approach has been developed theoretically[149] and has the potential to enable far-field super resolution for IR or Raman imaging using nanoprobes.

INCREASING ANALYTICAL CAPABILITY

As with most analytical techniques, the primary trade-offs in IR imaging involve data quality and acquisition time. Data metrics include spectral and spatial resolution and SNR as well as spatial and spectral coverage. Any of these can be changed to obtain data of different characteristics. In general, we recommend a “fit for purpose” approach. Whenever possible, the experiments should be planned in a manner that the required information can be obtained from the poorest quality of recorded data. Once the characteristics of the data to be recorded are known, a temporal limit can be found. There are several important means to affect this trade-off that are described next.

Discrete Frequency IR Imaging.

By the time point IR microscopy dawned in the 1980s, IR spectroscopy was almost exclusively recorded using interferometers and spatially and spectrally extended sources. The idea of a full spectrum was ingrained in acquisition (there is little advantage to collecting a narrow bandwidth in FT-IR spectroscopy) and analysis of data (full spectral methods were believed to provide greater accuracy). The idea of a using only a few frequencies for analysis[150] stems from the fact that the wealth of information may originate from the same molecules but in different modes. Therefore, the spectral variables are highly correlated and contain similar information, albeit with different variation and SNR.[151] As a result, the majority of applications of IR imaging can be performed with a smaller subset of frequencies; this has been shown in many classification approaches, where as little as 10−20% of the full set of variables are required for high accuracy.[35,152,153] Therefore, it is possible to design systems optimized to acquire only the critical frequencies in a rapid fashion. As opposed to FT-IR spectroscopy in which hundreds to thousands of contiguous data points are acquired over a wide bandwidth, this new approach is termed discrete frequency IR (DFIR) for its ability to measure narrowband responses at multiple spectral positions. A more detailed review of this idea in the field of IR and Raman imaging is available.[9] Here, we emphasize the analytical trade-offs in such an approach. Compared to FT-IR imaging systems (Figure 6), DFIR systems offer to change the acquisition and analysis of data. A relatively straightforward way to achieve a DF source is to use narrowband optical filters, which limit the bandwidth of the incoming beam[7] by reflecting only a selected portion of frequencies from a broadband globar source. Guided mode

resonance filters (GMRF)[73] and guided-mode-type Fano resonances (GFRs)[154] can achieve a narrow line width ($\lambda_{peak}/\Delta\lambda \sim 100$) and high reflectance values above a 70% range with a high peak-background contrast. A proof of principle imaging of biological samples has also been shown paving the way for practical applications of this approach.[75] However, the most critical factor is the low SNR. The weak thermal source is highly effective in an FT spectrometer as the broad bandwidth and efficiency of the FT approach make measurements possible. With the loss of the throughput and multiplexing advantages and the spread of light over a large area in imaging, the SNR of filtered thermal sources decreases substantially. Thus, the need for extensive signal averaging makes them impractical for rapid imaging.

Apart from an increase in the IR power, a QCL allows DF data acquisition,[9] especially for applications in which successful classification may not require the full mid-IR spectrum.[155] The scanning speed increase of a QCL microscope in a wide field configuration can reach a factor of 1000[38] per essential frequency as compared to an FT-IR system, while for a QCL point system, a factor of 180 was recently reported.[31] The increased speed can be used to scan much larger areas such as large polymer samples, pharmaceutical tablets, or forensic scenes and pieces of evidence.[156–160] An example of the DF potential in visualizing crystallization patterns of a polyethylene glycol (PEG) polymer over a large spatial region is shown in Figure 7. As can be seen (left panel), a ratio of just two frequencies (1415:1410 cm^{-1}) was enough to visualize the spherulite structure present in the PEG sample in just 9 min. QCLs, as most discrete sources likely will also have, offer a built-in linear polarization measurement due to the laser source. Using multiple polarizations and calculating an in-plane Herman's orientation function, it is possible to quantitatively visualize the orientation within single spherulites of a thick polymer sample in a simple and comparable ease by commonly using visible-cross polarized images (Figure 7, right panel). Orientation information can be obtained using only one frequency with 5 different polarization orientations, allowing much faster acquisition than a corresponding FT-IR approach. Even with the fastest QCL system available, there are reactions and processes whose time scales will still be elusive to study. The idea of spatially orienting the reaction pathway along with the imaging approach allows one to study the fast reaction and has already been developed in, e.g., microfluidic devices.[56,161–168] Such arrangements allow observation of processes happening on the submillisecond scale,[162] i.e., a mixing time of 269 μs. The coupling of accessories with IR imaging systems has been a relative rarity. We anticipate that the use of microfluidic systems, the ability to visualize dynamic changes, and the push toward live cell imaging will likely lead to a significant growth in both the use of innovative sampling accessories and new insight into problems that were not amenable to FT-IR imaging. In applications where speed or coverage is more important than extensive spectral detail, we anticipate that DFIR imaging approaches will rapidly gain acceptance.

High Intensity Sources.

The simplest, but expensive in components and design, approach to disrupting trade-offs is to use a brighter source and to proportionally increase SNR. One complication may be beam heating, but commonly available powers are insufficient to cause appreciable heating in thin samples with proper experimental design. The high intensity lends itself to multichannel detection as well. High intensity sources are also closely coupled to the use of multichannel

detectors. The advent of FPA detectors nearly two decades ago provided a much higher acquisition speed compared to then-extant single point detectors that were used in conjunction with apertures to restrict light. The multichannel detection advantage was so great that better data could be acquired using a multichannel detector with a thermal source than could be acquired by a synchrotron source-based point mapping system.[169] The higher throughput of synchrotrons could be utilized with an FPA detector to improve throughput in HD systems;[64] since then, coupling of FPAs into the optical setups at beamlines along with high definition capabilities (which require a significant amount of flux) again now offer an advantage over benchtop, thermal source, FT-IR imaging spectrometers. In almost all of the new IR beamlines, an FPA detector is installed, and the need for these is on the rise.[13,170] With QCLs, much larger format and uncooled detectors could be used. Similarly, point mapping with a QCL and small apertures is now much more effective and faster. Thus, the source has a profound effect on the spectrometer design and performance. New sources are driving new configurations, and more innovations can be expected from this transformation in IR imaging.

Sample Effects: Scattering from Heterogeneous Samples and Impacts of the Substrate.

One long-standing tenet, which is well validated for conventional homogeneous samples in IR spectral analysis, is that radiation that did not pass through the sample to the detector is largely absorbed. The absorption then is quantitatively related to concentration of chemical constituents through the Lambert−Beer law.[171] In microscopically heterogeneous samples and with limited collection angles of microscope optics, refractive index mismatches at interfaces lead to light scattering out of the collection volume of the objective.[7] This attenuation cannot be distinguished from molecular absorption in routine experiments and presents a complex interplay between morphology, material properties, optical configuration, and wavelength. In the case of simple geometries, such behavior is now understood and can be modeled from first principles.[172,173] A multilayer film can be analyzed easily; however, when the geometry of the interfaces is different from planar, the scattering profile has a more complicated shape. As a result, the scattering contribution to the absorption spectrum is convoluted with the measured spectrum and is observed as a complex deformation of a typical spectrum of a given material.[174] In the case of spherical objects and interfaces, the scattering contribution can completely dominate the spectrum, as has been shown for tissue samples for which scattering from a sphere is often cited as a model.[175] The prediction of spectral responses of morphologically and chemically varying systems remains a subject of much interest. One approach has been proposed to model samples as being composed of n- species and[176] try to model the entire response of composite materials. The number of species can be related to the analytical question. This need for using the recorded data, motivated by an understanding from first-principles and informed by the analytical problem, is likely to motivate many new computational approaches and remain a fertile ground for progress.

The rigorous electro-magnetic theory-based analysis in refs 172 and 173 allows for a variety of phenomena to be explained. One is the interference between light reflected and scattered from the different interfaces in transmission−reflection experiments, i.e., from the sample −air, within the sample, and the sample−substrate interface. The dimensions of the sample

and morphologic units are typically of the order of wavelength; hence, there is extensive electromagnetic coupling both in the far field and in the evanescent field. Further, synchrotron or laser beams have large coherence lengths. Hence, the general case for analyzing transflection data is complicated with coherent and incoherent, near-field and far-field additions. A special case of this has been termed electric field standing wave effect.[177–179] Most noticeably, since cells and tissue section thicknesses are in the 0.1−20 μm range, which is on the same order as the structured electric field, significantly altered band ratios[172,173,177–180] for the same material of different thickness can be observed. However, other studies have claimed that the magnitude of the effect in typical biological samples is small enough not to obscure details of the spectral differences between different components of tissues, for example, and it does not prevent creation of diagnostic methods in transflection mode of measurements.[179,181–185] Progress toward a greater understanding of the effect from theory[180,186–189] and careful analysis of the structure of low-e substrate as well as its reflective properties has been made. Interestingly, the magnitude of the distortion has been theoretically modeled and confirmed experimentally to be larger than for a gold substrate.[190] Similar analyses with coherent source systems have shown a large effect as well,[190] and the data are available for analysis.

From the discussion above, it is clear that there are multiple factors influencing a “simple” IR measurement and the resulting spectra depend heavily on the optical system. Only by rigorously understanding all of the factors in play, it is possible to gain real control of the system and push it to or even beyond its limits. Such control is best achieved by using theoretical approaches, and a proper model has been derived from first-principles for an IR imaging system.[172,173,191] This fundamental description allows one to investigate in detail effects coming into play in an imaging geometry, which would be hard to achieve and manipulate experimentally. Moreover, such a description can be used to optimize sampling requirements for achieving maximal spatial resolution as has been done and led to the development of high definition IR imaging.[98] We anticipate that theory and simulation driven design for IR imaging systems will gain greater traction with both the availability of these theoretical frameworks and the availability of newer (more economical) systems and components.

New Optical Configurations.

The availability of new understanding and new components is already starting to produce a diversity of instrumentation that was not available five years ago. A good example of experimental parameters optimization driven by theory was done by looking at the objective and condenser positions and the central obscuration size influence on deviation of a scattering sphere.[192] These parameters influence the effective NA of the system, which has significant impact on the acquired spectra. Moreover, it is apparent that the typical FT-IR configuration may not provide the optimal set of parameters for obtaining the most informative spectral signature. Another experimental approach was aimed at minimizing chromatic aberration caused by thick CaF_2 windows in a flow cell by introducing additional optical elements on the top and bottom of the windows to form a pseudohemisphere.[193–195] Such an approach not only forces all of the different light wavelengths to focus in one spot but also additionally increases the effective NA of the system, allowing more efficient light

collection and reducing scattering contributions to the recorded spectra. Another aspect of imaging is not to push the limits of pixel size but to expand the field of view and enable new applications. An interesting coupling of ATR with the microfluidics has been recently reported,[161] which avoids the requirement of IR light transmitting through both sample and the device, enabling one to study the dissolution of tablets and resulting ibuprofen concentration gradients, for example (Figure 8). However, even in this instance, there is a limit of probing only a portion of the system due to evanescent wavelength, which is in the order of a few micrometers. With the advent of lasers and demonstration of standoff systems, it is likely that macro imaging standoff configurations will soon be reported. We anticipate that there will be systems that cover nano to meter scale spectroscopic imaging, with versatile instruments considerably blurring the distinction between capabilities and opening new analytical opportunities. The commonality of components between these diverse instruments, at the same time, will drive costs lower. The increased availability of many components at lower costs spurring new designs and the theoretical and computational tools will spur instrumentation innovation and new analytical capabilities.

Inverse Problems and Computational Advances.

While significant progress has been made in modeling the recorded data from known sample properties (the forward problem), a significant focus now lies in solving the inverse problem, i.e., predicting the sample parameters (IR optical properties and morphology) based only on the spectral response. At this point, an arbitrarily heterogeneous sample of variable geometry is too complex to be properly solved from first principles. Hence, the quest for solving the inverse problem has focused rightly on simple geometries. A spherical sample is the most logical starting point since the scattering functions for spherical objects are well-defined and validated under a variety of conditions. Successfully recovering an absorption spectrum from a polymer sphere measured in an IR microscope has been developed[93] and became a foundation for later methods. With similar developments for other geometries (e.g., cylinders) and integration with advanced computational tools, it is significantly easier now to understand structure−spectra relationships. Extension of single particle to multiparticle systems and, eventually, complex samples has also been recently proposed. An interesting result is that increasing spatial coverage by particles converges the spectrum to steady change that depends only on the volume fraction akin to an effective medium approach.[196] The volumetric coverage was, interestingly, found to be similar to the percolation thresholds observed for conductivity development, for example, high-lighting the correlation between IR response and broader electromagnetic properties of materials. Another direction[92,95] has been to additionally use information expanding from the traditional mid-IR range of 800−4000 cm^{-1} up to 8000 cm^{-1}. These regions not only allow the analysis to take advantage of a low-absorbing region with broad (slowly varying) spectral features to make inversions more consistent but also contain increased scattering information from smaller objects and finer refractive index discontinuities in the sample. An interesting direction that is likely to emerge is well illustrated by the work of Kohler and co-workers[91,94,95,197] starting from basic scattering ideas and adapted to microscopy parameters and integrated with computing algorithms. Such an approach, with a diversity of models to account for spatial and spectral structures, holds great promise in extending the forward model to corrected data for applications.

SELECTED APPLICATIONS OF IR CHEMICAL IMAGING

Applications of IR imaging have expanded rapidly in the past few years. A large majority of applications are in the biomedical domain, and we especially focus on describing several interesting directions of the same. An exceptional collection of studies on different applications, some underlying technology,[198–202] and lively integrated discussions[203–206] has been published as part of a report on a Faraday Discussions meeting. Recent reviews, as mentioned previously, in biomedical sciences, plants, polymers, and forensics remain relevant. Here, we focus on selected recent advances in biomedical sciences to illustrate the directions of progress in this field.

Advances in Biomedical Imaging: Conventional Imaging Analyses.

By the label of conventional imaging, we distinguish those studies not taking advantage of HD capabilities. These studies consist of the majority of the work being currently done, partly due to the recent introduction of HD imaging and partly due to its challenges in application (the smaller pixel size may not be needed, long acquisition times, low SNR). The well-established technology is being used to answer several important questions for applications. One issue concerns the preparation method for biosamples since removal of cells or tissues from their bodily environment will necessarily cause chemical changes. The assumption that the same procedure should give roughly the same chemical changes to different cell lines and tissue samples was tested by Verdonck et al.[207] using formalin-fixation and paraffin-embedding (FFPE). Four breast cancer and four melanoma cell lines were measured before and after FFPE, and an effect on the spectral signatures was found. A similarity measure between the cell lines was identified to be quite well preserved and maintained classification potential indicating that the procedure is not preventing accurate discrimination. Discrimination between different lymphocyte subpopulations was shown to be possible on cells isolated from peripheral blood of healthy donors.[208,209] These include successful distinction between helper T cells, cytotoxic T cells, regulatory T cells, and B cells. Also, esophageal cells isolated from a patient were successfully identified as squamous, Barret’s, or dysplastic.[210] These studies illustrate the robustness of IR data under varying conditions, but the ability is likely different for other cell types and problems. Thus, both the activities toward understanding optics and biologically induced variance in data are needed. We anticipate that the exploration of the consistency of IR signals and their dependence on experimental variables is likely to be a continuing trend in applications. This direction will only speed up with HD optics leading to a different convolution between the morphology and pixel size as well as coherent sources being applied at fewer frequencies to these samples. The challenge will be to recognize and quantify variance arising from different factors, to control it, or to mitigate its effects on scientific conclusions.

Exquisite biochemical IR sensitivity was observed by Cao et al.[184] in human embryonic stem cells phenotype caused by tissue culturing conditions, which persisted even upon differentiation toward mesoendodermal lineages. This study illustrates the potential of IR imaging to be used as a noninvasive screening tool. A study by Smolina and Goormaghtigh[211] investigated whether 3D culturing conditions create a better environment than a traditional 2D culturing geometry for simulating breast cancer. It was found that 3D

grown colonies can be distinguished from 2D grown cells by using a supervised method (while unsupervised did not discriminate fully) and that by comparing the spectral signatures to those obtained from a patient the 3D grown more closely resembled the actual tumor signature. Sarkar et al.[212] observed stimulated epithelial-to-mesenchymal transition of lung normal and cancerous lung cell lines. Gaydou et al.[213] reported a lung tumor cell line invasiveness scale based on IR imaging based on a relative scale assigned to four different cell lines. These studies are important to pursue since they address the question of whether biochemical fate of cells and tissues can be predicted by early observations. As opposed to stains or dyes in which the precise nature of molecular transformation must be known, the use of IR imaging not only is label-free but also may afford sensitivity to change that arises from a nonspecific knowledge of the precise molecular transformations. Wrobel et al.[214] reported the influence of ATR crystal contact on the state of a single endothelial cell, while Gaigneaux and Goormaghtigh[215] showed that by controlling the ATR depth of penetration it is possible to increase the discrimination power between chemoresistant and sensitive K562 cell lines. These studies illustrate the use of sampling geometry to enable or enhance analyses of cells. It is important to recall that many sampling modes and accessories exist for bulk IR spectroscopy as different applications have different needs. Similarly, the concurrent demonstration of need from application areas and the development of new instrumentation discussed previously can be highly synergistic.

In tissue analysis (histology) by IR imaging, several exciting developments focused on using extended spectral and spatial features to not only detect different cell units but provide significant detail on major problems such as disease subclassification, drug response, and quantification of major biological processes. In breast cancer, more powerful imaging results included combination of spectral and spatial features for cancer detection using tissue microarrays[153] and a comprehensive histopathology along with cancer detection on biopsies.[216,217] Melanoma studies reported identification of melanoma cells in primary tumors;[218] however, no clear distinction between non-and metastatic lesions was found. When patients were grouped into 2 groups, i.e., early stage (I and II) and late stage (III and IV), spectral distinction could be made. The information contained in the primary seems to be sufficient to predict chemotherapy response[219] to dacarbazine. Melanoma cells were also successfully identified in lymph node metastases.[220] Progress in accurate subtyping of lung cancer[221] using multilevel Random Forest classification was also reported along with improved colon cancer grading.[222] Liver progression through fibrosis, cirrhosis, dysplasia, and hepatocellular carcinoma[223] were studied by FT-IR imaging. Quantification of liver fat in a nonalcoholic fatty liver[224] was reported, and quantification of chemical changes induced by atherosclerosis progression[225,226] and by a low carbohydrate, high protein diet in atherosclerotic tissue was also performed.[227,228] Also, changes in murine brain induced by atherosclerosis were observed in both white and gray matter[229] mostly related to protein to lipid ratio and presence of cholesterol. Brain ischemic changes were detected, and a method of simultaneous semiquantification of glycogen and lactate was developed.[230] The major histologic changes in cardiac tissue transplant success were also found to be predicted using IR imaging.[231] Sinonasal lesions were analyzed in order to detect inflammatory sinonasal polyps, benign Schneiderian papillomas, and sinonasal undifferentiated carcinomas.[232] Discrimination of healthy and osteoarthritic articular cartilages[233] and intervertebral disc

degeneration[234] was successfully observed using IR imaging. A new carbon hydroxyapatite/β-glucan composite for bone tissue engineering[235] and structural transformation of synthetic hydroxyapatite[236] were both studied showing the potential of IR imaging in the biomaterials field. Together, these examples illustrate strongly that IR imaging can be applied for a variety of tissues and problems. The advances in applications provide impetus for the development of new analytical methods, faster analysis, and more capable instrumentation. A key development in the coming years will be the development and translation of instrumentation appropriate for a specific problem. Major issues that are outstanding include the need to scan faster for rapid coverage of large areas, development of robust data handling protocols, and widespread testing.

Live Cell Imaging.—A vast majority of applications of IR imaging are of dry, fixed tissue. While informative, studies on static biological materials only provide limited information and processing may obscure some dynamic changes. Hence, live cell imaging is highly desirable but very challenging. Water often constitutes 70−90% of the path length in live cell imaging setups, even in optimally designed experiments. Since water has very strong absorbance modes in the mid-IR, it swamps spectra of cells and tissues. Moreover, IR data is recorded using transmitted light, which is highly diminished by the strong water absorbance resulting in low light throughput and low SNR. One avenue is to use ATR imaging such that the problem of large path lengths and throughput can be avoided. Applications of ATR imaging for live cell imaging have been recently described in depth[237] and will not be covered here. We highlight an important consideration in dynamic imaging, namely, that of determining the dynamic levels of chemicals of interest. An estimate of the sensitivity limits for measuring the chemical constituents has been determined to be around 20 μM,[238] which corresponds to a monolayer of proteins[239] for general IR spectroscopy. This limits the number of actually detected chemicals and can be compared to concentrations of some of a living cell chemical species as is shown in Figure 9. These components do not represent any particular cellular state but are a compiled list of typical human metabolites and their cytoplasmic concentrations. We anticipate that, with the smaller volumes and high performing IR microscopes, this limit can routinely be exceeded today. In particular, the higher throughput and discrete frequencies of laser sources will allow the limit to be exceeded in neat samples or unique or when the compound can be identified. The analytical challenge often, however, is to extract these components from a background of similar chemicals. In complex analytical backgrounds, the use of advanced mathematical techniques becomes critical and is applied on a case by case basis.

Spatial and Molecular Detail To Probe the Microenvironment and Microchemical Changes in Cancer.—While significantly lower concentrations can be detected by other methods (e.g., single molecule quantification by scanning probe or fluorescent techniques), the quantification limit of IR imaging will ultimately be limited by sensitivity of measurement and time. The strength of IR spectroscopic imaging, however, lies in simultaneously measuring multiple chemical species and in measuring the same in a spatially resolved sense. Most importantly, sensitive changes in concentrations of multiple species can be used as a pattern of change that is specific to physiologic transformations. Though limited in the molecular identity of contributors, this useful information cannot be

obtained otherwise. For example, a recent study examined prostate cancer recurrence prediction[240] using IR imaging and compared the prediction ability to two established methods based on histopathology (CAPRA-S and KATTAN) in a case control study of difficult cases. The results are shown in Figure 10, and it can be seen that the IR-based approach outperformed both of these methods in providing a measure of the risk in predicting lethal prostate cancer upon initial diagnosis. Moreover, data mining using frequent pattern matching revealed that the features giving the predictive power were located in the stroma adjacent to the tumor. The power of IR imaging in rapidly assessing functional state of tissues and key chemical changes that can be followed up by other tools is a major strength. A combination of different techniques can provide both additional data and a complementary view. IR and Raman imaging together have a multitude of applications from atherosclerotic tissue[229 ,241–244] or cells[245] up to a combination with other techniques, such as atomic force microscopy,[244] mass spectrometry,[246] visible,[247] or laser capture micro-dissection followed by proteomics.[248] The last study by Großerueschkamp et al.[248] is an excellent example of the convergence of the initial examination by IR imaging followed by detailed proteomic analysis using biotechnology tools. Such an integrated approach allows for the exceptional levels of spatial and spectral detail to be obtained. In this study, FT-IR imaging resolves tumor subtypes within tissue sections in an automated manner with ~85% accuracy for diffuse malignant mesothelioma (DMM) subtypes. Since the tissue is highly heterogeneous, IR imaging was used to identify small regions of interest without the need for human supervision. Subsequently, the identified regions were image registered and dissected as homogeneous samples using laser capture microdissection. This material is now available for conventional biological analysis in an automated, likely quantitative, and unbiased sampling manner. While proteomic analysis in general for a large tissue section may be difficult, this preanalytical focusing allowed subsequent proteome analysis to provide informative, location-specific molecular detail. The study could identify 142 differentially expressed proteins, including five protein biomarkers commonly used in DMM immunohistochemistry panels. This is an exceptional result in demonstrating the power of IR imaging to inform conventional biochemical assays. Relation of proteomic profiles back to IR data may allow for future “one step” spatial and molecular detail. The utility of IR imaging in resolving morphological alterations as well as specific molecules (here, proteins) augers well for its use in -omic studies to focus analytical tools and analyses that are otherwise expensive or can get confounded by tissue heterogeneity. Finally, the fully automated workflow of this study is exemplary in demonstrating how IR imaging-guided analysis can enable efficiency, automation, and objectivity of the assay in predictive biomarkers research and clinical use.

While the example studies above provide rigorous analysis of both the direct application of IR imaging and its use for precise molecular analysis and potential clinical translation, there remains much to understand on the basic level of cellular transformations and interactions of cells with their micro-environment. Extending the illustrations above to other possibilities, IR imaging offers several interesting directions where the biological changes are complex in molecular and spatial detail: (a) detecting chemical changes without prior knowledge of molecular changes, thereby aiding discovery in spatially heterogeneous systems (*where* to perform analyses), (b) dynamic assessment of changes in materials where the time course

may not be known (*when* to perform analyses), (c) sensitivity of chemical changes to analytical methods (*impact* of performing analyses), and (d) a potential corroboration of alternate methods of analyses by other techniques (*how* to perform analyses). Holton et al.[249] studied the cross-talk between fibroblasts and estrogen-positive breast cancer cells in a 3D culture model. It was found that fibroblasts induce epithelial-to-mesenchymal transition in the cancer cells leading to a more invasive phenotype and resistance to endocrine therapy, which could be detected spectroscopically. A study focusing on the effect of different cell lines directly on tumor microenvironment phantoms has found significant changes associated with collagen in the case of invading melanoma and carcinoma cells[250] and rather small changes for 4 different breast cancer cell lines also related with collagen. Such a result again confirms the potential of IR imaging and shows much promise for future applications in automated and sensitive analysis of heterogeneous research materials.

Stainless Staining.—While IR imaging is an information rich technique and provides molecular details, most analyses have focused on using the information content to provide an independent view of tissue information (e.g., by color coded images). While these images are easy to understand, relation of IR data to existing histopathologic knowledge is desirable to relate to the knowledge base of pathology and to relate to views familiar to practitioners and to provide information so that it can be readily adopted. IR data was used for computationally recreating histological staining results in a technique termed “digital staining”.[251] The central idea is to provide images that illustrate common staining patterns such as for hematoxylin and eosin (H&E) as well as other molecular entities that are useful but may not be routine from a cost perspective. Stainless staining not only prevents sample changes during chemical staining, preserving it better for downstream biological analyses as illustrated above, but also provides an added advantage of acquiring overlapping information on the same tissue slice. This is crucial if multiple stains are required to make a diagnostic decision or inform research and consecutive sections do differ in morphological detail. While initial studies have shown potential for some of the common stains in breast tissue, the limits of information that can be extracted from an IR image have not yet been reached. We anticipate that greater molecular detail will be available in a variety of tissues and disease types.

Advances in Biomedical Imaging: Emerging Technologies.

HD FT-IR Laboratory Studies.—As mentioned above, one major need is to enhance spatial detail in IR imaging to be competitive with optical imaging. The increase in image detail provided by HD IR is a great improvement for tissue imaging,[100] for single cell imaging[99] and, potentially, for complex classification purposes. With the smaller pixel sizes, however, there is also risk that additional variability may limit the potential of the technique to create accurate models of the tissue histopathology. Such behavior was observed for lymphatic tissue;[102] however, this problem was overcome with a supervised and robust Random Forest classification algorithm. A complex, 8 class model was created, able to distinguish naive and memory B cells, T cells, light zone activated B cells, and dark zone activated B cells. Recent preliminary results using HD optics also show that prostate tissue classification does not suffer from a decrease in accuracy.[101] An example of increasing specificity by the use of HD optics was also recently shown in a study of colon tissue,

allowing discrimination of goblet cells along with their mucin secretions.[103,252] Breast tissue analysis using HD has also been shown,[253] followed by the creation of a more complex tissue structure classification.[35] HD imaging has also helped in identification of parasites in single erythrocytes[107] by increasing spatial resolution of the parasite signal and in observing tendon damage using linearly polarized light.[106] All these studies point cautiously to the idea that improved computational methods may be able to overcome variability in data that may arise from smaller pixels. One mitigating factor is that the longer wavelengths may imply that the same information (weighted slightly differently) is present in pixels, thus smoothing out chemical changes and offering a prodigious compromise between high spatial detail and consistent spectral detail. When needed, visualization methods can then be tuned to enhance local spatial contrast to provide sharper edges while the gradual chemical changes can be used to provide consistent recognition of cell identity and physiologic changes. Clearly, when pixels are smaller than the wavelength, significant effects will arise from the broad bandwidth of IR spectra. These effects have not been explored or used in classification. This interplay between spatial detail and spectral content as well as its effect on analytical capability will gather some attention in the future. Nevertheless, HD optics provide a level of spatial detail that is close to routine optical microscopy in performance (factor of ~4 larger, as opposed to ~100 in pixel area) providing a quality that may be acceptable for many research and clinical purposes.

Synchrotron Studies.—Synchrotrons have pioneered IR microscopy and imaging experiments with the first HD experiments[64] followed by other applications including first 3D tomographic reconstruction,[65] first confocal IR microscope,[254] super hydrophobic wing surface chemistry,[255] and time-lapsed[256] or disease related[257] changes in protein structure. Due to their high brilliance, synchrotron centers were also a place of microfluidics development[56,164] and single cell[105] or other biosamples[170] analysis. The development of new beamlines and many dedicated IR imaging centers augurs well for this trend to continue and drive major innovations in IR microscopy. A particularly encouraging sign has been the transition from synchrotron to laboratory use of many of these techniques. While relatively expensive to maintain, the impact of synchrotron sources on the development of IR imaging and as a measurement resource for many applications has been exceptional. We anticipate that this trend will continue in the near future.

QCL Studies.—The field of QCL imaging is on the verge of exponential growth due to first commercially available QCL microscopes and demonstrations of new capabilities. New applications in biomedical research[258] include studies of colon,[40,41,259] breast,[38,260] heart,[231] prostate,[261] and brain[30] tissues. Moreover, examples include imaging of biofluids either of serum[30,262] or of protein solutions.[43,263] An example of the discrete frequency approach using QCL imaging has recently been demonstrated in identification of fibrosis[264] within human cardiovascular samples. A similar idea was incorporated on fibrotic liver tissue.[265] Finally, first measurements of a live organism[39] and surface enhanced infrared absorption (SEIRA)[266] are also available, providing new dimensions to IR imaging. While new applications are rapidly becoming available, specific experimental protocols are also being developed. For example, in a study aimed at optimizing QCL measurements in aqueous solutions, an optimal path length of water has been found to be 20 μm when SNR was

optimized. An SNR of above 10 was still maintained for thicknesses up to 100 μm depending on the frequency used,[263] a depth of analysis unimaginable with the weak globar sources in FT-IR imaging. In another study using a QCL microscope, a limit of detection (LOD) of 3 μg/cm^2 of dried serum sample was reported.[262] A more recent study reported cancer screening capabilities of this approach correctly detecting brain, breast, lung, and skin cancer samples.[32] While instrumentation development, often in a fit for purpose approach, is obviously a major direction, new applications are likely to emerge as well. New computational strategies, especially those geared toward translation of continuous spectra to discrete frequencies, are needed. A framework to optimize information with SNR, measurement time, and limited number of frequencies will alter the basic trade-offs in measurements, requiring careful optimization for each experiment. Thus, there will be a trend not only for tailored instrumentation but also for experiments that are carefully designed to take advantage of the unique ability of DF measurements using QCLs to alter the analytical performance to the needs of the practitioner.

CONCLUSIONS

IR imaging is experiencing a fast and broad development both in the technology and in fundamental understanding of the technique driving the experimental progress. Imaging on macro-, micro-, and nanoscales is now feasible, especially with QCL-based microscopes paving the way for ultrafast measurements and screening. We anticipate a much greater diversity of instrumentation with the availability of new components and of theory to achieve novel results. One offshoot of the developments over the past few years has been to renew interest in IR imaging and provide new challenges in instrument and experimental design as well as analysis of data. We emphasize that integration of instrumentation, acquisition, and analysis is now possible to an extent that is fundamentally different than practice in the past. This presents a rich and powerful analytical opportunity for a variety of fields of study, especially in the biomedical sciences.

ACKNOWLEDGMENTS

Research reported in this Review was supported by the National Cancer Institute of the National Institutes of Health under award 5R01CA197516. The content is solely the responsibility of the authors and does not necessarily represent the official views of the National Institutes of Health. T.P.W. was supported by a Beckman Institute Postdoctoral Fellowship from the Beckman Institute for Advanced Science and Technology, University of Illinois at Urbana−Champaign. T.P.W. is now supported from the “Pancreatic cancer comprehensive histopathology based on IR chemical imaging” project, which is carried out within the Homing programme of the Foundation for Polish Science cofinanced by the European Union under the European Regional Development Fund.

Biographies

Tomasz P. Wrobel is an Assistant Professor at the Institute of Nuclear Physics Polish Academy of Sciences in Krakow (Poland). During his graduate studies (supervisor Prof. Malgorzata Baranska) at the Faculty of Chemistry (Jagiellonian University), he was also a research assistant in Jagiellonian Centre for Experimental Therapeutics (JCET) working with Prof. Stefan Chlopicki. In 2013, he was a recipient of the William G. Fateley Stent Award. Afterwards, he was awarded a Beckman Institute Postdoctoral Fellowship (2014−2017) by the University of Illinois at Urbana−Champaign and joined the lab of Prof.

Rohit Bhargava. His research interests are focused on chemical imaging techniques applied to biomedical problems with a special emphasis on infrared (IR) imaging and machine learning in cancer research.

Rohit Bhargava is a Bliss Faculty Scholar and Founder Professor of Engineering in the Bioengineering Department (with affiliate appointments in Chemical and Biomolecular Engineering, Mechanical Science and Engineering, Electrical and Computer Engineering, and Chemistry). He received a dual B. Tech. degree (Chemical Engineering with a minor in Polymer Science and Engineering) from the Indian Institute of Technology, New Delhi, and doctoral degree from Case Western Reserve University. After a stint at the National Institutes of Health, Rohit has been at Illinois as Assistant Professor (2005−2011), Associate Professor (2011−2012), and Professor (2012−present). Rohit has pioneered the development of infrared spectroscopic imaging, starting from his doctoral thesis that was the first in this field. Fundamental work in theory and numerical methods in his laboratory directly leads to new instrumentation and technologies. Instruments developed in his laboratory have been used to provide new means to characterize and define cancer using chemical imaging that are leading to the emergence of the field of digital molecular pathology. Using 3D printing and engineered tumor models, his most recent research seeks to create designer cancers in the laboratory. Rohit founded and serves as the Director of the Cancer Center at Illinois, a University-wide effort dedicated to advancing cancer-related research and scholarship at Illinois. The effort is a unique approach to oncology across the lifespan and the first such national center combining high quality engineering with the field of oncology. Earlier in his career, Rohit was among the first faculty in the new Bioengineering Department at Illinois and played a key role in its development.

REFERENCES

(1). Lewis EN; Treado PJ; Reeder RC; Story GM; Dowrey AE; Marcott C; Levin IW Anal. Chem 1995, 67 (19), 3377–3381. [PubMed: 8686889]

(2). Colarusso P; Kidder LH; Levin IW; Fraser JC; Arens JF; Lewis EN Appl. Spectrosc 1998, 52 (3), 106A–120A.

(3). Snively CM; Katzenberger S; Oskarsdottir G; Lauterbach J Opt Lett 1999, 24 (24), 1841. [PubMed: 18079949]

(4). Huffman SW; Bhargava R; Levin IW Appl. Spectrosc 2002, 56 (8), 965–969.

(5). Bhargava R; Levin IW Appl Spectrosc 2003, 57 (4), 357–366. [PubMed: 14658631]

(6). Bhargava R; Levin IW Spectrochemical Analysis Using Infrared Multichannel Detectors; Sheffield Analytical Chemistry Series; Wiley: New York, 2008.

(7). Bhargava R Appl Spectrosc 2012, 66 (10), 1091–1120. [PubMed: 23031693]

(8). Levin IW; Bhargava R Anna. Rev. Phys. Chem 2005, 56 (1), 429–474. [PubMed: 15796707]

(9). Wrobel TP; Kole MR; Bhargava R Spectroscopy 2016, 31 (6).

(10). Baker MJ; Trevisan J; Bassan P; Bhargava R; Butler HJ; Dorling KM; Fielden PR; Fogarty SW; Fullwood NJ; Heys KA; Hughes C; Lasch P; Maitin-Hirsch PL; Obinaju B; Sockalingum GD; Sule-Suso J; Strong RJ; Walsh MJ; Wood BR; Gardner P; Martin FL Nat Protoc 2014, 9 (8), 1771–1791. [PubMed: 24992094]

(11). Kazarian SG; Chan KLA Analyst 2013, 138 (7), 1940–1951. [PubMed: 23400222]

(12). Bhargava R; Wang S; Koenig JL Adv. Polym. Sd 2003, 163, 137–191.

(13). Ellis GJ; Martin MC Ear. Polym. J 2016, 81, 505–531.

(14). Gierlinger N Appl. Spectrosc Rev 2017, 4928, 1–35.

(15). Chalmers JM; Howell GM; Edwards MDH Infrared and Raman Spectroscopy in Forensic Science; Wiley: New York, 2012.

(16). Diem M; Griffiths PR; Chalmers JM Vibrational spectroscopy for medical diagnosis; John Wiley & Sons: New York, 2008; Vol. 40.

(17). Pilling M; Gardner P Chem. Soc. Rev 2016, 45 (7), 1935–1957. [PubMed: 26996636]

(18). Doherty J; Cinque G; Gardner P Appl. Spectrosc. Rev 2017, 52 (6), 560–587.

(19). Miller LM; Dumas P Biochim. Biophys. Acta, Biomembr 2006, 1758 (7), 846–857.

(20). Griffiths PR; De Haseth JA Fourier Transform Infrared Spectrometry; Wiley-Interscience: New York, 2007.

(21). Sorokina IT; Vodopyanov KL Solid-state mid-infrared laser sources; Springer Science & Business Media: New York, 2003.

(22). Schliesser A; Picque N; Hansch TW Nat Photonics 2012, 6 (7), 440–449.

(23). Jackson SD Nat. Photonics 2012, 6 (7), 423–431.

(24). Nader N; Maser DL; Cruz FC; Kowligy A; Timmers H; Chiles J; Fredrick C; Westly DA; Nam SW; Mirin RP; Shainline JM; Diddams SA arXiv Prepr. arXivl707.03679 2017, 1–26.

25. () Lavoute L; Sandt C; Borondics F; Ducros N; Fevrier S In Specialty Optical Fibers; Academic Press: Boston, 2016; Vol. 2016, p SoTu2G-5.

(26). Yao Y; Hoffman AJ; Gmachl C Nat. Photonics 2012, 6, 432–439.

(27). Zhou W; Wu D; McClintock R; Slivken S; Razeghi M Optica 2017, 4 (10), 1228.

(28). Kole MR; Reddy RK; Schulmerich MV; Gelber MK; Bhargava R Anal Chem 2012, 84 (23), 10366–10372. [PubMed: 23113653]

(29). Yeh K; Schulmerich M; Bhargava R Proc. SPIE 2013, 8726 (217), 87260E.

(30). Clemens G; Bird B; Weida M; Rowlette J; Baker MJ Spectrosc Ear 2014, 26, 14–19.

(31). Wrobel TP; Mukherjee P; Bhargava R Analyst 2017, 142 (1), 75–79.

(32). Hughes C; Clemens G; Bird B; Dawson T; Ashton KM; Jenkinson MD; Brodbelt A; Weida M; Fotheringham E; Barre M; Rowlette J; Baker MJ Sci. Rep 2016, 6, 20173. [PubMed: 26842132]

(33). Maulini R; Beck M; Faist J; Gini E Appl. Phys. Lett 2004,84 (10), 1659–1661.

(34). Liu X; Chae I; Miriyala N; Lee D; Thundat T; Kim S Appl. Spectrosc 2017, 71 (7), 1494–1505. [PubMed: 28664781]

(35). Mittal S; Wrobel TP; Leslie S; Kadjacsy-Balla A; Bhargava R In Progress in Biomedical Optics and Imaging - Proceedings of SPIE; Gurcan MN., Madabhushi A, Eds.; International Society for Optics and Photonics: Bellingham, WA, 2016; Vol. 9791, pp 1–8.

(36). Kimber JA; Kazarian SG Anal. Bioanal. Chem 2017, 409 (25), 5813. [PubMed: 28852781]

(37). Ogunleke A; Bobroff V; Chen HH; Rowlette J; Delugin M; Recur B; Hwu Y; Petibois C TrAC, Trends Anal. Chem 2017, 89, 190–196.

(38). Yeh K; Kenkel S; Liu J-N; Bhargava R Anal. Chem 2015, 87 (1), 485–493. [PubMed: 25474546]

(39). Haase K; Kroger-Lui N; Pucci A; Schonhals A; Petrich WJ Biophotonics 2016, 9 (1–2), 61–66. [PubMed: 26572683]

(40). Kroger-Lui N; Gretz N; Haase K; Kränzlin B; Neudecker S; Pucci A; Regenscheit A; Schonhals A; Petrich W Analyst 2015, 140 (7), 2086–2092. [PubMed: 25649324]

(41). Kröger N; Egl A; Engel M; Gretz N; Haase K; Herpich I; Kranzlin B; Neudecker S; Pucci A; Schonhals A; Vogt J; Petrich WJ Biomed. Opt 2014, 19, 111607.

(42). Haka AS; Levin IW; Lewis EN Appl. Spectrosc 2000, 54 (5), 753–755.

(43). Alcaraz MR; Schwaighofer A; Kristament C; Ramer G; Brandstetter M; Goicoechea H; Lendl B Anal. Chem 2015, 87 (13), 6980–6987. [PubMed: 26059222]

(44). Alcaraz MR; Schwaighofer A; Goicoechea H; Lendl B Anal Bioanal Chem 2016, 408 (15), 3933–3941. [PubMed: 27007739]

(45). Hanrer A; Szedlak R; Schwarz B; Moser H; Zederbauer T; MacFaiiand D; Detz FL; Andrews AM; Schrenk W; Lendl B; Strasser G Sci Rep 2016, 6, 21795. [PubMed: 26887891]

(46). Schwaighofer A; Alcaraz MR; Araman C; Goicoechea H; Lendl B Sci. Rep 2016, 6, 33556. [PubMed: 27633337]

(47). Tütüncü E; Kokoric V; Szedlak R; MacFarland D; Zederbauer T; Detz H; Andrews AM; Schrenk W; Strasser G; Mizaikoff B Analyst 2016, 141 (22), 6202–6207. [PubMed: 27508281]

(48). Haas J; Stach R; Sieger M; Gashi Z; Godejohann M; Mizaikoff B Anal. Methods 2016, 8 (36), 6602–6606.

(49). Sieger M; Haas J; Jetter M; Michler P; Godejohann M; Mizaikoff B Anal. Chem 2016, 88 (5), 2558–2562. [PubMed: 26845392]

(50). Reffner JA; Martoglio PA; Williams GP Rev. Sci. Instrum 1995, 66 (2), 1298–1302.

(51). Rowlette J; Weide M; Bird B; Amone D; Barre M; Day T BioOptics World 2014, 7 (2), 34–37.

(52). Bhargava R; Levin IW Spectrochemical Analysis Using Infrared Multichannel Detectors; Bhargava R, Levin IW, Eds.; Blackwell Publishing Ltd: Oxford, UK, 2005.

(53). Stavitski E; Smith RJ; Bourassa MW; Acerbo AS; Carr GL; Miller LM Anal. Chem 2013, 85 (7), 3599–3605. [PubMed: 23458231]

(54). Carr GL; Miller LM; Dumas P In Biomedical Applications of Synchrotron Infrared Microspectroscopy, Royal Society of Chemistry: Cambridge, 2010; pp 226–259.

(55). Hirschmugl CJ; Gough KM Appl. Spectrosc 2012, 66 (5), 475–491. [PubMed: 22524953]

(56). Loutherback K; Birarda G; Chen L; Holman HN Protein Pept Lett 2016, 23 (1), 273–282. [PubMed: 26732243]

(57). Holman H-YN; Bjomstad KA; McNamara MP; Martin MC; McKinney WR; Blakely EAJ Biomed. Opt 2002, 7 (3), 417.

(58). Holman H-YN; Martin MC; McKinney WR Spectroscopy 2003, 17, 139–159.

(59). Holman H-YN; Hao Z; Martin MC; Bechtel HA Synchrotron Radial News 2010, 23 (5), 12–19.

(60). Moss DA; Keese M; Pepperkok R Vilb. Spectrosc 2005, 38 (1–2), 185–191.

(61). Holman HYN; Miles R; Hao Z; Wozei E; Anderson LM; Yang H Anal Chem 2009, 81 (20), 8564–8570. [PubMed: 19775125]

(62). Birarda G; Grenci G; Businaro L; Marmiroli B; Pacor S; Vaccari L Microelectron. Eng 2010, 87 (5—8), 806–809.

(63). Kaun N; Kulka S; Frank J; Schade U; Vellekoop MJ; Harasek M; Lendl B Analyst 2006, 131 (4), 489–494. [PubMed: 16568164]

(64). Nasse MJ; Walsh MJ; Mattson EC; Reininger R; Kajdacsy-balla A; Macias V; Bhargava R; Hirschmugl CJ Nat. Methods 2011, 8 (5), 413–418. [PubMed: 21423192]

(65). Martin MC; Dabat-Blondeau C; Unger M; Sedlmair J; Parkinson DY; Bechtel HA; Illiman B; Castro JM; Keiluweit M; Buschke D; Ogle B; Nasse MJ; Hirsdimugl CJ Nat Methods 2013, 10 (9), 861–864. [PubMed: 23913258]

(66). Ritter E; Puskar L; Aziz EF; Hofmann K-P; Hegemann P; Schade U In 2017 42nd International Conference on Infrared, Millimeter, and Terahertz Waves (IRMMW-THz), Aug 27 to Sept 1, 2017; IEEE: New York, pp 1–2.

(67). Michaelian K; Kelley C; Pedersen T; Frogley M; May T; Quaroni L; Cinque G; Tg A arXiv Prepr. arXivl706.09844 2017, 1–4.

(68). Masson A; O'Brien JT; Williams ER; Holman H-YN Synchrotron Radial News 2017, 30 (4), 17–23.

(69). Tanino K; Willick I; Hamilton K; Vijayan P; Jiang Y; Brar GS Can. J. Plant Sci 2017, 996, 1–40.

(70). Faye M; Bordessoule M; Kanoute B; Brubach J-B; Roy P; Manceron L Rev. Sci. Instrum 2016, 87 (6), 063119. [PubMed: 27370438]

(71). Bechtel HA; Muller EA; Olmon RL; Khatib O; Martin MC; Raschke MB Fourier Transform Spectrosc 2016, FTu2E-l.

(72). Bechtel HA; Muller EA; Olmon RL; Martin MC; Raschke MB Proc. Natl. Acad. Sci. U. S A 2014, 111 (20), 7191–7196. [PubMed: 24803431]

(73). Kodali AK; Schulmerich M; Ip J; Yen G; Cunningham BT; Bhargava R Anal. Chem 2010, 82 (13), 5697–5706. [PubMed: 20527738]

(74). Liu J-N; Schulmerich MV; Bhargava R; Cunningham BT Opt Express 2011, 19 (24), 24182. [PubMed: 22109445]

(75). Liu J-N; Schulmerich MV; Bhargava R; Cunningham BT Opt InfoBase Conf. Pap 2014, 5–6.

(76). Petersen CR; Moller U; Kubat I; Zhou B; Dupont S; Ramsay J; Benson T; Sujecki S; Abdel-Moneim N; Tang Z; Furniss D; Seddon A; Bang O Nat Photonics 2014, 8 (11), 830–834.

(77). Møller U; Yu Y; Kubat I; Petersen CR; Gai X; Brilland L; Méchin D; Caillaud C; Troles J; Luther-Davies B; Bang O Opt Express 2015, 23 (3), 3282. [PubMed: 25836186]

(78). Yu Y; Gai X; Wang T; Ma P; Wang R; Yang Z; Choi DY; Madden S; Luther-Davies B Opt. Mater. Express 2013, 3 (8), 1075–1086.

(79). Ouyang D; Zhao J; Zheng Z; Liu M; Li C; Ruan S; Yan P; Pei J IEEE Photonics J 2016, 8 (3), 1600910.

(80). Swiderski J Prog. Quantum Electron 2014, 38 (5), 189–235.

(81). Petersen CR; Engelsholm RD; Markos C; Brilland L; Caillaud C; Troles J; Bang O Opt. Express 2017, 25 (13), 15336–15347. [PubMed: 28788961]

(82). Pedersen C; Tidemand-Lichtenberg P Nonlinear Frequency Generation and Conversion: Materials, Devices, and Applications XV; SPIE: Bellingham, WA, 2016; Vol. 9731, pp 1–5.

(83). Johnson TA; Diddams SA Appl. Phys. B: Lasers Opt 2012, 107 (1), 31–39.

(84). Dam JS; Tidemand-Lichtenberg P; Pedersen C Nat Photonics 2012, 6 (11), 788–793.

(85). Katzenmeyer AM; Holland G; Kjoller K; Centrone A Anal. Chem 2015, 87 (6), 3154–3159. [PubMed: 25707296]

(86). Hugi A; Villares G; Blaser S; Liu HC; Faist J Nature 2012, 492 (7428), 229–233. [PubMed: 23235876]

(87). Jouy P; Faist J In CLEO: Applications and Technology 2017; 2017; pp 3–4.

(88). Lu Q; Wu D; Slivken S; Razeghi M Sci. Rep 2017, 7, 43806. [PubMed: 28262834]

(89). Berisha S; Chang S; Saki S; Daeinejad D; He Z; Mankar R; Mayerich D Analyst 2017, 142 (8), 1350–1357. [PubMed: 27924319]

(90). Mayerich D; Walsh M; Schulmerich M; Bhargava R BMC Bioinf 2013, 14, 156.

(91). Konevsldkh T; Ponossov A; Blumel R; Lukacs R; Kohler A Analyst 2015, 140 (12), 3969–3980. [PubMed: 25893226]

(92). Lukacs R; Blumel R; Zimmerman B; Bagaoglu M; Kohler A Analyst 2015, 140 (9), 3273–3284. [PubMed: 25797528]

(93). Van Dijk T; Mayerich D; Carney PS; Bhargava R Appl. Spectrosc 2013, 67 (5), 546–552. [PubMed: 23643044]

(94). Konevsldkh T; Lukacs R; Blumel R; Ponossov A; Kohler A Faraday Discuss 2016, 187, 235–257. [PubMed: 27034998]

(95). Blumel R; Bagcioglu M; Lukacs R; Kohler A J. Opt. Soc. Am. A 2016, 33 (9), 1687.

(96). Bassan P; Kohler A; Martens H; Lee J; Jackson E; Lockyer N; Dumas P; Brown M; Clarke N; Gardner PJ Biophotonics 2010, 3 (8–9), 609–620. [PubMed: 20414907]

(97). Berisha S; van Dijk T; Bhargava R; Camey PS; Mayerich D Front Phys 2017, 5, 5. [PubMed: 29170738]

(98). Reddy RK; Walsh MJ; Schulmerich MV; Camey PS; Bhargava R Appl Spectrosc 2013, 67 (1), 93–105. [PubMed: 23317676]

(99). Hughes C; Henderson A; Kansiz M; Dorling K; Jimenez-Hemandez M; Brown MD; Clarke NW; Gardner P Analyst 2015, 140 (140), 2080–2085. [PubMed: 25738183]

(100). Findlay CR; Wiens R; Rak M; Sedlmair J; Hirschmugl CJ; Morrison J; Mundy CJ; Kansiz M; Gough KM Analyst 2015, 140 (140), 2493–2503. [PubMed: 25600495]

(101). Wrobel TP; Kwak JT; Kadjacsy-balla A; Bhargava R Proc SPIE 2016, 97911D.

(102). Leslie LSS; Wrobel TPTP; Mayerich D; Bindra S; Emmadi R; Bhargava R PLoS One 2015, 10 (6), e0127238. [PubMed: 26039216]

(103). Nallala J; Lloyd GR; Shepherd N; Stone N Analyst 2016, 141 (141), 630–639. [PubMed: 26549223]

(104). Sreedhar H; Varma VK; Nguyen PL; Davidson B; Akkina S; Guzman G; Setty S; Kajdacsy-Balla A; Walsh MJ J. Visualized Exp 2015, e52332.

(105). Mattson EC; Unger M; Clede S; Lambert F; Policar C; Imtiaz A; D'Souza R; Hirschmugl CJ Analyst 2013, 138 (19), 5610–5618. [PubMed: 23826609]

(106). Wiens RA; Findlay CRJ; Baldwin SGJ; Kreplak L; Lee JM; Veres SP; Gough KM Faraday Discuss 2016, 187, 555–573. [PubMed: 27048856]

(107). Perez-Guaita D; Andrew D; Heraud P; Beeson J; Anderson D; Richards JS; Wood BR Faraday Discuss 2016, 187, 341–352. [PubMed: 27071693]

(108). Vamivakas AN; Younger RD; Goldberg BB; Swan AK; Ünlü MS; Behringer ER; Ippolito SB Am. J. Phys 2008, 76 (8), 758–768.

(109). Ippolito SB; Goldbeig BB; Unlii MS Appl. Phys. Lett 2001, 78 (26), 4071–4073.

(110). Reddy RK; Bhargava R Analyst 2010, 135 (11), 2818–2825. [PubMed: 20830324]

(111). Zhang D; Li C; Zhang C; Slipchenko MN; Eakins G; Cheng J-X ScL Adv 2016, 2 (9), e1600521.

(112). Li Z; Kuno M; Haitland G Proc. SPIE 2015, 9549, 954912.

(113). Totachawattana A; Regan MS; Agar NYR; Erramilli S; Sander MY CLEO Appl. Technol.2017 2017, 1, ATu4A.3.

(114). Totachawattana A; Erramilli S; Sander MY Proc. SPIE 2016, 99560Y.

(115). Totachawattana A; Erramilli S; Sander MY Proc. SPIE 2015, 95840C.

(116). Gaiduk A; Ruijgrok PV; Yorulmaz M; Orrit M Chem. Sci 2010, 1 (3), 343.

(117). Nedosekin DA; Galanzha EI; Dervishi E; Biris AS; Zharov VP Small 2014, 10 (1), 135–142. [PubMed: 23864531]

(118). Boyer D; Tamarat P; Maali A; Lounis B; Orrit M Science (Washington, DC, U S.) 2002, 297 (5584), 1160–1163.

(119). van Dijk T; Mayerich D; Bhargava R; Camey S Opt. Express 2013, 21 (10), 12822–12830. [PubMed: 23736501]

(120). Amenabar I; Poly S; Goikoetxea M; Nuansing W; Lasch P; Hillenbrand R Nat. Commun 2017, 8, 14402. [PubMed: 28198384]

(121). Mastel S; Govyadinov AA; de Oliveira TVAG; Amenabar I; Hillenbrand R Appl. Phys. Lett 2015, 106 (2015), 023113.

(122). Taubner T; Hillenbrand R; Keilmann F Appl. Phys. Lett 2004, 85 (21), 5064–5066.

(123). Qin N; Zhang S; Jiang J; Corder SG; Qian Z; Zhou Z; Lee W; Liu K; Wang X; Li X; Shi Z; Mao Y; Bechtel HA; Martin MC; Xia X; Marelli B; Kaplan DL; Omenetto FG; Liu M; Tao TH Nat Commun 2016, 7, 13079. [PubMed: 27713412]

(124). Govyadinov AA; Amenabar I; Huth F; Scott Camey P.; Hillenbrand RJ Phys. Chem. Lett 2013, 4 (9), 1526–1531.

(125). Marcott C; Lo M; Kjoller K; Fiat F; Baghdadli N; Balooch G; Luengo GS Appl. Spectrosc 2014, 68 (5), 564–569. [PubMed: 25014600]

(126). Ruggeri FS; Longo G; Faggiano S; Lipiec E; Pastore A; Dietler G Nat Commun 2015, 6, 7831. [PubMed: 26215704]

(127). Li AG; Burggraf LW; Xing Y Appl. Environ. Microbiol 2016, 82 (10), 2988–2999. [PubMed: 26969703]

(128). Hau H; Khanal D; Rogers L; Suchowerska N; Kumar R; Sridhar S; McKenzie D; Chrzanowski W Bioeng. Transl. Med 2016, 1, 94–103. [PubMed: 29313009]

(129). Vitry P; Rebois R; Bourillot E; Deniset-Besseau A; Virolle MJ; Lesniewska E; Dazzi A Nano Res 2016, 9 (6), 1674–1681.

(130). Barlow DE; Biffinger JC; Cockrell-Zugell AL; Lo M; Kjoller IC; Cook D; Lee WK; Pehrsson PE; Crookes-Goodson WJ; Hung C-S; Nadeau LJ; Russell JN Analyst 2016, 141, 4848–4854. [PubMed: 27403761]

(131). Ruggeri FS; Vieweg S; Cendrowska U; Longo G; Child A; Lashuel HA; Dietler G Sci Rep 2016, 6, 31155. [PubMed: 27499269]

(132). Giliberti V; Baldassarrc L; Rosa A; de Turns V; Ortolani M; Calvani P; Nucara A Nanoscale 2016, 8 (40), 17560–17567. [PubMed: 27714081]

(133). Baldassarrc L; Giliberti V; Rosa A; Ortolani M; Bonamore A; Baiocco P; Kjoller K; Calvani P; Nucara A Nanotechnology 2016, 27 (7), 075101. [PubMed: 26778320]

(134). Janik E; Bednarska J; Zubik M; Puzio M; Luchowski R; Grudzinski W; Mazur R; Garstka M; Maksymiec W; Kulik A; Dietler G; Gruszecki WI Plant Cell 2013, 25, 2155–2170. [PubMed: 23898030]

(135). Harrison AJ; Bilgili EA; Beaudoin SP; Taylor LS Anal. Chem 2013, 85 (23), 11449–11455. [PubMed: 24171582]

(136). Marcott C; Lo M; Kjoller K; Domanov Y; Balooch G; Luengo GS Exp. Dermatol 2013, 22 (6), 419–421. [PubMed: 23651342]

(137). Müller T; Ruggeri FS; Kulik AJ; Shimanovich U; Mason TO; Knowles TPJ; Dietler G Lab Chip 2014, 14 (7), 1315–1319. [PubMed: 24519414]

(138). Deniset-Besseau A; Prater CB; Virolle M-J; Dazzi A J. Phys. Chem. Lett 2014, 5 (4), 654–658. [PubMed: 26270832]

(139). Wood BR; Bambery KR; Evans CJ; Quinn M. a.; McNaughton D BMC Med. Imaging 2006, 6 (12), 1–9. [PubMed: 16630362]

(140). Quaroni L; Obst M; Nowak M; Zobi F Angew. Chem., Int Ed 2015, 54 (1), 318–322.

(141). Chan KLA; Tay FH; Poulter G; Kazarian SG Appl. Spectrosc 2008, 62 (10), 1102–1107. [PubMed: 18926019]

(142). Chan KLA; Kazarian SG Appl. Spectrosc 2007, 61 (1), 48–54. [PubMed: 17311716]

(143). Wrobel TPTP; Vichi A; Baranska M; Kazarian SG Appl. Spectrosc 2015, 69 (10), 1170–1174. [PubMed: 26449810]

(144). Petibois C Trends Biotechnol 2017, 35, 1194–1207. [PubMed: 28893404]

(145). Lasch P; Naumann D Biochim. Biophys. Acta, Biomembr 2006, 1758 (7), 814–829.

(146). Offroy M; Roggo Y; Milan far P; Duponchel L Anal. Chim. Acta 2010, 674 (2), 220–226. [PubMed: 20678633]

(147). Piqueras S; Duponchel L; Offroy M; Jamme F; Tauler R; de Juan A Anal. Chem 2013, 85 (13), 6303–6311. [PubMed: 23697511]

(148). Mattson E; Nasse MJ; Hirschmugl CJ In Microscopy and Microanalysis; 2010; Vol. 16, pp 764–765. [PubMed: 20920389]

(149). Van Dijk T; Mayerich D; Bhargava R; Scott Carney P. Opt Express 2013, 21 (10), 12822–12830. [PubMed: 23736501]

(150). Lloyd GR; Stone N Appl. Spectrosc 2015, 69 (9), 1066–1073. [PubMed: 26253762]

(151). Kwak JT; Reddy R; Sinha S; Bhargava R Anal Chem 2012, 84 (2), 1063–1069. [PubMed: 22148458]

(152). Bhargava R; Fernandez DC; Hewitt SM; Levin IW Biochim. Biophys. Acta, Biomembr 2006, 1758 (7), 830–845.

(153). Pounder FN; Reddy RK; Bhargava R Faraday Discuss 2016, 187 (0), 43–68. [PubMed: 27095431]

(154). Liu J-N; Schulmerich MV; Bhargava R; Cunningham BT Opt Express 2014, 22 (15), 18142–18158. [PubMed: 25089433]

(155). Tiwari S; Bhargava R Yale J. Biol. Med 2015, 88 (2), 131–143. [PubMed: 26029012]

(156). Sugawara S; Nakayama Y; Taniguchi H; Ishimaru I Sci.Rep 2017, 7 (1), 12395. [PubMed: 28963529]

(157). Ewing AV; Kazarian SG Analyst 2017, 142 (2), 257–272. [PubMed: 27905577]

(158). Fuchs F; Hugger S; Jarvis J; Yang QK; Ostendorf R; Schilling C; Bronner W; Driad R; Aidam R; Wagner J Proc. SPIE 2016, 983621.

(159). Galan-Freyle NJ; Pacheco-Londono LC; Roman-Ospino AD; Hemandez-Rivera SP Appl. Spectrosc 2016, 70 (9), 1511–1519. [PubMed: 27558366]

(160). Li C; Zhang D; Slipchenko MN; Cheng JX Anal. Chem 2017, 89 (9), 4863–4867. [PubMed: 28398722]

(161). Ewing AV; Clarke GS; Kazarian SG Biomicrofluidics 2016, 10 (2), 024125. [PubMed: 27158293]

(162). Rise DP; Magana D; Reddish MJ; Dyer RB Lab Chip 2014, 14 (3), 584–591. [PubMed: 24302515]

(163). Birarda G; Ravasio A; Suryana M; Maniam S; Holman HYN; Grenci G Lab Chip 2016, 16, 1644–1651. [PubMed: 27040369]

(164). Silverwood IP; Al-Rifai N; Cao E; Nelson DJ; Chutia A; Wells PP; Nolan SP; Frogley MD; Cinque G; Gavrülidis A; Catlow CRA Rev. Sci. Instrum 2016, 87 (2), 024101. [PubMed: 26931867]

(165). Barich MV; Krummel AT Anal Chem 2013, 85 (21), 10000–10003. [PubMed: 24099528]

(166). Polshin E; Verbraggen B; Witters D; Sels B; De Vos D; Nicolai B; Lammertyn J Sens. Actuators, B 2014, 196, 175–182.

(167). Fagaschewski J; Sellin D; Wiedenhofer C; Bohne S; Trieu HK; Hilterhaus L Bioprocess Biosyst. Eng 2015, 38, 1399–1405. [PubMed: 25732540]

(168). Ryu M; Kimber JA; Sato T; Nakatani R; Hayakawa T; Romano MJ Pradere C; Hovhannisyan AA; Kazarian SG; Morikawa J Chem. Eng. J 2017, 324, 259–265.

(169). Miller LM; Smith GD; Carr GL J.Biol. Phys 2003, 29, 219–230. [PubMed: 23345838]

(170). Marcelli A; Cricenti A; Kwiatek WM; Petibois C Biotechnol. Adv 2012, 30 (6), 1390–1404. [PubMed: 22401782]

(171). Mohlenhoff B; Romeo M; Diem M; Wood BR Biophys. J 2005, 88 (5), 3635 −3640. [PubMed: 15749767]

(172). Davis BJ; Carney PS; Bhargava R Anal. Chem 2010, 82 (9), 3474–3486. [PubMed: 20392063]

(173). Davis BJ; Carney PS; Bhargava R Anal. Chem 2010, 82 (9), 3487–3499. [PubMed: 20392064]

(174). Miljkovic M; Bird B; Diem M Analyst 2012, 137 (17), 3954–3964. [PubMed: 22811966]

(175). Bassan P; Byrne HJ; Lee J; Bonnier F; Clarke C; Dumas P; Gazi E; Brown MD; Clarke NW; Gardner P Analyst 2009, 134 (6), 1171–1175. [PubMed: 19475144]

(176). Deutsch B; Reddy R; Mayerich D; Bhargava R; Carney PS J. Opt. Soc. Am. A 2015, 32 (6), 1126.

(177). Filik J; Frogley MD; Pijanka JK; Wehbe K; Cinque G Analyst 2012, 137 (4), 853–861. [PubMed: 22231204]

(178). Bassan P; Lee J; Sachdeva A; Pissardini J; Dorling KM; Fletcher JS; Henderson A; Gardner P Analyst 2013, 138, 144–157. [PubMed: 23099638]

(179). Wrobel TPTP; Wajnchold B; Byrne HJHJ; Baranska M Vib. Spectrosc 2013, 69, 84–92.

(180). Mayerhofer TG; Popp J Spedrochim. Acta, Part A 2018, 191, 283–289.

(181). Wrobel TP; Wajnchold B; Byrne HJ; Baranska M Vib. Spedrosc 2014, 71, 115.

(182). Kochan K; Heraud P; Kiupel M; Yuzbasiyan-Gurkan V; Mcnaughton D; Baranska M; Wood BR Analyst 2015, 140 (7), 2402–2411. [PubMed: 25502543]

(183). Perez-Guaita D; Heraud P; Marzec KM; de la Guardia M; Kiupel M; Wood BR Analyst 2015, 140 (7), 2376–2382. [PubMed: 25695358]

(184). Cao J; Ng ES; McNaughton D; Stanley EG; Elefanty AG; Tobin MJ; Heraud P Analyst 2013, 138 (14), 4147–4160. [PubMed: 23745179]

(185). Pilling MJ; Bassan P; Gardner P Analyst 2015, 140 (7), 2383–2392. [PubMed: 25672838]

(186). Mayerhofer TG; Popp J Spedrochim. Acta, Part A 2018, 191, 165–171.

(187). Mayerhofer TG; Mutschke H; Popp J ChemPhysChem 2017, 18 (20), 2916–2923. [PubMed: 28771914]

(188). Hendaoui N; Mani A; Liu N; Tofail SM; Silien C; Peremans A Opt Commun 2017, 382, 574–579.

(189). Lee J Vib. Spectrosc 2017, 90, 104–111.

(190). DeVetter BMBM; Kenkel S; Mittal S; Bhargava R; Wrobel TPTP Vib. Spedrosc 2017, 91, 119–127.

(191). Davis BJ; Carney PS; Bhargava R Anal. Chem 2011, 83 (2), 525–532. [PubMed: 21158469]

(192). Mayerich D; van Dijk T; Walsh MJ; Schulmerich MV; Carney PS; Bhargava R Analyst 2014, 139 (16), 4031–4036. [PubMed: 24936526]

(193). Chan KLA; Kazarian SG Anal. Chem 2013, 85 (2), 1029–1036. [PubMed: 23244035]

(194). Kimber JA; Foreman L; Turner B; Rich P; Kazarian SG Faraday Discuss 2016, 187, 69–85. [PubMed: 27056467]

(195). Dougan JA; Kazarian SG Spectrosc. Eur 2013, 25 (5), 6–12.

(196). Rasskazov IL; Spegazzini N; Carney PS; Bhargava R Anal Chem 2017, 89 (20), 10813–10818. [PubMed: 28895722]

(197). Konevskikh T; Lukacs R; Kohler A J. Biophotonics 2017, e201600307.

(198). Diem M; Ergin A; Remiszewski S; Mu X; Akalin A; Raz D Faraday Discuss 2016, 187, 9–42. [PubMed: 27075634]

(199). Quaroni L; Zlateva T; Wehbe K; Cinque G Faraday Discuss 2016, 187, 259–271. [PubMed: 27049435]

(200). Lovergne L; Bouzy P; Untereiner V; Gamotel R; Baker MJ; Thiefin G; Sockalingum GD Faraday Discuss 2016, 187, 521–537. [PubMed: 27048927]

(201). Meade AD; Howe O; Unterreiner V; Sockalingum GD; Byrne HJ; Lyng FM Faraday Discuss 2016, 187, 213–234. [PubMed: 27043923]

(202). Amrania H; Drummond L; Coombes RC; Shousha S; Woodley-Barker L; Weir K; Hart W; Carter I; Phillips CC Faraday Discuss 2016, 187 (0), 539–553. [PubMed: 27077445]

(203). Goodacre R; Sergo V; Barr H; Sammon C; Schultz ZD; Baker MJ; Graham D; Marques MP; Sulé-Suso J; Livermore J; Faulds K; Sinjab F; Matousek P; Campbell CJ; Dluhy R; Gardner P; Phillips C; Diem M; Wood B; Apolonskiy A; Kazarian S; Fullwood L; Gough K; Petrich W; Lloyd G; Ibrahim O; Cinque G; Sockalingum GD; Stone N; Kendall C; McAughtrie S; Perez-Guaita D; Clark L; Gerwert K; Bonifacio A; Notingher I; Lasch P; Bhargava R; Lepert G; Mader K; Paterson C Faraday Discuss 2016, 187, 429–460. [PubMed: 27282545]

(204). Baker MJ; Goodacre R; Sammon C; Marques MP; Gardner P; Tipping W; Sulé-Suso J; Wood B; Byme HJ; Hermes M; Matousek P; Campbell CJ; El-Mashtoly S; Frost J; Phillips C; Diem M; Kohler A; Lau K; Kazarian S; Petrich W; Lloyd G; Delfino I; Cinque G; Isabelle M; Stone N; Kendall C; Jamieson L; Perez-Guaita D; Clark L; Gerwert K; Notingjier I; Quaroni L; Bhargava R; Meade A; Lyng F Faraday Discuss 2016, 187, 299–327. [PubMed: 27282416]

(205). Sammon C; Schultz ZD; Kazarian S; Barr H; Goodacre R; Graham D; Baker MJ; Gardner P; Wood B; Campbell CJ; Dluhy R; El-Mashtoly S; Phillips C; Frost J; Diem M; Kohler A; Haris P; Apolonskiy A; Amrania H; Lasch P; Zhang Z; Petrich W; Sockalingum GD; Stone N; Gerwert K; Notingher I; Bhargava R; Kröger-Lui N; Isabelle M; Pilling M Faraday Discuss 2016, 187, 155–186. [PubMed: 27282288]

(206). Goodacre R; Baker MJ; Graham D; Schultz ZD; Diem M; Marques MP; Cinque G; Vemooij R; Sulé-Suso J; Byme HJ; Faulds K; Hermes M; Fleming H; Bonifacio A; Dluhy R; Gardner P; El-Mashtoly S; Wood B; Gough K; Fornasaro S; Kazarian S; Jamieson L; Petrich W; Sockalingum GD; Stone N; Kendall C; Sinjab F; Haris P; Subaihi A; Remiszewsld S; Hellwig P; Sergo V; Gerwert K; Phillips C; Campbell CJ Faraday Discuss 2016, 187 (0), 575–601. [PubMed: 27282657]

(207). Verdonck M; Wald N; Janssis J; Yan P; Meyer C; Legat A; Speiser DE; Desmedt C; Larsimont D; Sotiriou C; Goormaghtigh E Analyst 2013, 138 (14), 4083–4091. [PubMed: 23689823]

(208). Wald N; Legat A; Meyer C; Speiser DE; Goormaghtigh E Analyst 2015, 140, 2257–2265. [PubMed: 25553786]

(209). Verdonck M; Garaud S; Duvillier H; Willard-Gallo K; Goormaghtigh E- Analyst 2015, 140, 2247–2256. [PubMed: 25516910]

(210). Townsend D; Miljkovix M; Bird B; Lenau K; Old O; Almond M; Kendall C; Lloyd G; Shepherd N; Barr FL; Stone N; Diem M Analyst 2015, 140 (7), 2215–2223. [PubMed: 25594077]

(211). Smolina M; Goormaghtigh E Analyst 2015, 140 (7), 2336–2343. [PubMed: 25568895]

(212). Sarkar A; Sengupta S; Mukherjee A; Chatterjee J Spectrochim. Acta, Part A 2017, 173, 809–816.

(213). Gaydou V; Polette M; Gobinet C; Kileztky C; Angiboust J-F; Manfait M; Birembaut P; Piot O Anal. Chem 2016, 88, 8459–8467. [PubMed: 27482917]

(214). Wrobel TP; Marzec KM; Majzner K; Kochan K; Bartus M; Chlopicki S; Baranska M Analyst 2012, 137 (18), 4135–4139. [PubMed: 22854681]

(215). Gaigneaux A; Goormaghtigh E Analyst 2013, 138 (14), 4070–4075. [PubMed: 23675579]

(216). Verdonck M; Denayer A; Delvaux B; Garaud S; De Wind R; Desmedt C; Sotiriou C; Willard-Gallo K; Goormaghtigh E Analyst 2016, 141, 606–619. [PubMed: 26535413]

(217). Bassan P; Mellor J; Shapiro J; Williams KJ; Lisanti MP; Gardner P Anal Chem 2014, 86 (3), 1648–1653. [PubMed: 24410403]

(218). Wald N; Goormaghtigh E Analyst 2015, 140 (140), 2144–2155. [PubMed: 25574519]

(219). Wald N; Le Corre Y; Martin L; Mathieu V; Goormaghtigh E Biodtim. Biophys. Acta, Mol Basis Dis 2016, 1862 (2), 174–181.

(220). Wald N; Bordry N; Foukas PGG; Speiser DEE; Goormaghtigh E Biodtim. Biophys. Acta, Mol Basis Dis 2016, 1862 (2), 202–212.

(221). Großeraeschkamp F; Kallenbach-Thieltges A; Behrens T; Brüning T; Altmayer M; Stamatis G; Theegarten D; Gerwert K Analyst 2015, 140 (140), 2114–2120. [PubMed: 25529256]

(222). Kuepper C; Großerüschkamp F; Kallenbach-Thieltges A; Mosig A; Tannapfel A; Gerwert K Faraday Discuss 2016, 187, 105–118. [PubMed: 27064063]

(223). Sreedhar H; Pant M; Ronquillo NR; Davidson B; Nguyen P; Chennuri R; Choi J; Herrera J. a.; Hinojosa AC; Jin M; Kajdacsy-Balla A; Guzman G; Walsh MJ Proc. SPIE 2014, 8939, 893901.

(224). Kochan K; Maslak E; Chlopicki S; Baranska M Analyst 2015, 140, 4997–5002. [PubMed: 26051164]

(225). Wrobel TP; Mateuszuk L; Kostogrys RB; Chlopicki S; Baranska M Analyst 2013, 138 (21), 6645. [PubMed: 24040642]

(226). Wrobel TP; Mateuszuk L; Chlopicki S; Malek K; Baranska M Analyst 2011, 136 (24), 5247–5255. [PubMed: 22007352]

(227). Wrobel TP; Marzec KM; Chlopicki S; Maslak E;Jasztal A; Franczyk-Zarów M; Czyzyńska-Cichoń I; Moszkowski T; Kostogrys RB; Baranska M Sa. Rep 2015, 5, 14002.

(228). Kostogrys RB; Johann C; Czyżyńska I; Franczyk-Żarów M; Drahun A; Maślak E; Jasztal A; Gajda M; Mateuszuk Ł; Wrobel TP; Baranska M; Wybrańska I; Jezkova K; Nachtigal P; Chlopicki SJ Nutr., Health Aging 2015, 19 (7), 710.

(229). Kochan K; Chrabaszcz K; Szczur B; Maslak E; Dybas J; Marzec KM Analyst 2016, 141, 5329–5338. [PubMed: 27332112]

(230). Hackett MJ; Sylvain NJ; Hou H; Caine S; Alaverdashvili M; Pushie MJ; Kelly ME Anal Chem 2016, 88 (22), 10949–10956. [PubMed: 27690391]

(231). Tiwari S; Reddy VB; Bhargava R; Raman J PLoS One 2015, 10 (5), e0125183. [PubMed: 25932912]

(232). Giorgini E; Sabbatini S; Conti C; Rnbini C; Rocchetti R; Re M; Vaceari L; Mitri E; Librando VJ Biomed. Opt 2015, 20 (12), 125003.

(233). Zhang X-X; Yin J-H; Mao Z-H; Xia YJ Biomed. Opt 2015, 20 (6), 060501.

(234). Mader K; Peeters M; Detiger S; Helder M; Smit T; Le Maitre C; Sammon C Faraday Discuss 2016, 187, 393–414. [PubMed: 27057647]

(235). Sroka-Bartnicka A; Kimber JA; Borkowski L; Pawlowska M; Polkowska I; Kalisz G; Belcarz A; Jozwiak K; Ginalska G; Kazarian SG Anal. Bbanal. Chem 2015, 407 (25), 7775–7785.

(236). Sroka-Bartnicka A; Borkowski L; Ginalska G; Ślósarczyk A; Kazarian SG Spectrochim. Acta, Part A 2017, 171, 155–161.

(237). Andrew Chan KL; Kazarian SG Chem. Soc. Rev 2016, 45, 1850–1864. [PubMed: 26488803]

(238). Chan KLA; Fale PLV Anal. Chem 2014, 86, 11673–11679. [PubMed: 25376865]

(239). De Meutter J; Derfoufi K-M; Goormaghtigh E Biomed. Spectrosc Imaging 2016, 5 (2), 145–154.

(240). Kwak JT; Kajdacsy-Balla A; Macias V; Walsh M; Sinha S; Bhargava R Sci. Rep 2015, 5, 8758. [PubMed: 25737022]

(241). Lattermann A; Matthäus C; Bergner N; Beleites C; Romeike BF; Krafft C; Brehm BR; Popp J J.Biophotonics 2013, 6 (1), 110–121. [PubMed: 23139154]

(242). Wrobel TP; Marzec KM; Chlopicki S; Maślak E; Jasztal A Sci. Rep 2015, 5, 14002. [PubMed: 26391802]

(243). Wróbel TP; Fedorowicz A; Mateuszuk L; Maślak E; Jasztal A; Chlopicki S; Marzec KM In Optical Spectroscopy and Computational Methods in Biology and Medicine, Baranska M, Ed.; Springer: Netherlands, 2014; pp 505–535.

(244). Marzec KM; Wrobel TP; Rygula A; Maslak E; Jasztal A; Fedorowicz A; Chlopicki S; Baranska MJ Biophotonics 2014, 7 (9), 744–756. [PubMed: 24604883]

(245). Perez-Guaita D; Kochan K; Martin M; Andrew DW; Heraud P; Richards JS; Wood BR Vilb. Spectrosc 2017, 91, 46–58.

(246). Masyuko R; Lanni EJ; Sweedler JV; Bohn PW Analyst 2013, 138 (7), 1924–1939. [PubMed: 23431559]

(247). Kwak JT; Hewitt SM; Sinha S; Bhargava R BMC Cancer 2011, 11 (1), 62. [PubMed: 21303560]

(248). Großerueschkamp F; Bracht T; Diehl HC; Kuepper C; Ahrens M; Kallenbach-Thieltges A; Mosig A; Eisenacher M; Marcus K; Behrens T; Brüning T; Theegarten D; Sitek B; Gerwert K Sci. Rep 2017, 7, 44829. [PubMed: 28358042]

(249). Holton SE; Bergamaschi A; Katzenellenbogen BS; Bhargava R PLoS One 2014, 9 (5), e96878. [PubMed: 24816718]

(250). Ukkonen H; Kumar S; Mikkonen J; Salo T; Singh SPP; Koistinen APP; Goormaghtigh E; Kullaa AMM Vih. Spectrosc 2015, 79, 24–30.

(251). Mayerich D; Walsh MJ; Kadjacsy-Balla A; Ray PS; Hewitt SM; Bhargava R Technology 2015, 3 (1), 27–31. [PubMed: 26029735]

(252). Nallala J; Lloyd GR; Hermes M; Shepherd N; Stone N Vib. Spectrosc 2017, 91, 83–91.

(253). Leslie LS; Kadjacsy-Balla A; Bhargava R Proc. SPIE 2015, 9420, 942001.

(254). Jamme F; Lagarde B; Giuliani A; Garcia GA; Mercury L J. Phys.: Conf. Ser 2013, 425 (14), 142002.

(255). Tobin MJ; Puskar L; Hasan J; Webb HK; Hirschmugl CJ; Nasse MJ; Gervinskas G; Juodkazis S; Watson GS; Watson J. a.; Crawford RJ; Ivanova EP J. Synchrotron Radiat 2013, 20 (3), 482–489. [PubMed: 23592628]

(256). Gelfand P; Smith RJ; Stavitski E; Borchelt DR; Miller L M Anal Chem 2015, 87 (12), 6025–6031.

(257). Hackett MJ; Smith SE; Caine S; Nichol H; George GN; Pickering IJ; Paterson PG Free Radical Biol. Med 2015, 89, 806–818. [PubMed: 26454085]

(258). Schwaighofer A; Brandstetter M; Lendl B Chem. Soc. Rev 2017, 46, 5903. [PubMed: 28816307]

(259). Bird B; Baker MJ Trends Biotechnol 2015, 33 (10), 557–558. [PubMed: 26409774]

(260). Bassan P; Weida MJ; Rowlette J; Gardner P Analyst 2014, 139, 3856–3859. [PubMed: 24965124]

(261). Pilling MJ; Gardner P; Henderson A; Brown MD; Bird B; Clarke NW Faraday Discuss 2016, 187, 135–154. [PubMed: 27095185]

(262). Mukherjee A; Bylund Q; Prasanna M; Margalit Y; Tihan TJ Biomed. Opt 2013, 18 (3), 036011.

(263). Haase K; Kröger-Lui N; Pucci A; Schönhals A; Petrich W Faraday Discuss 2016, 187, 119–134. [PubMed: 27032367]

(264). Tiwari S; Raman J; Reddy V; Ghetler A; Telia RP; Han Y; Moon CR; Hoke CD; Bhargava R Anal. Chem 2016, 88 (20), 10183–10190. [PubMed: 27626947]

(265). Bird B; Rowlette J Analyst 2017, 142, 1179–1184. [PubMed: 27858020]

(266). Hasenkampf A; Kröger N; Schönhals A; Petrich W; Pucci A Opf. Express 2015, 23 (5), 5670.

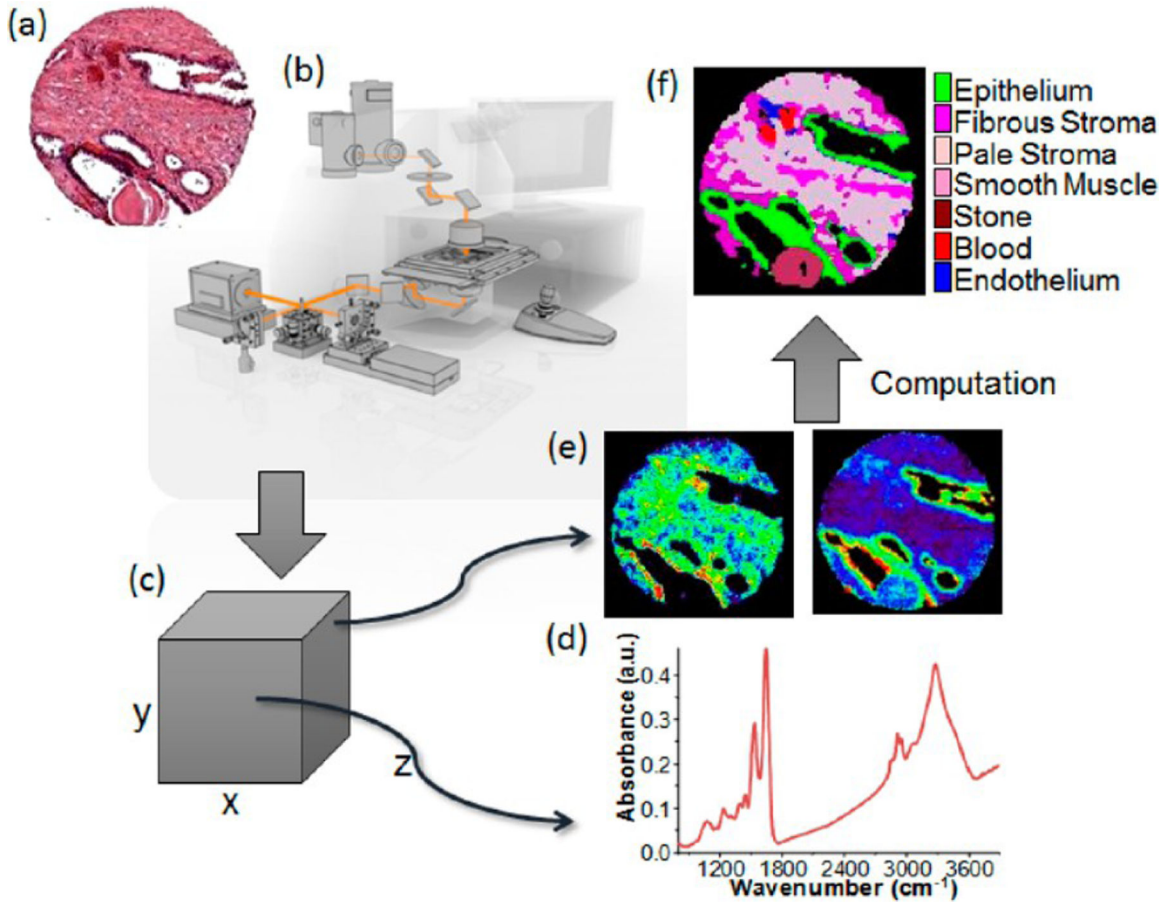

Figure 1.

Illustration of the potential of IR imaging in biomedical analysis. (a) A typical H&E stained section of prostate tissue in which cellular recognition is achieved by specific morphologies. (b) The optical layout of a typical FT-IR spectrometer, comprised of a spectrometer, microscope, and computer. (c) A “three-dimensional” data set is obtained from an imaging measurement containing typical biological absorption spectra (d) which can be used to visualize different chemical components based on the absorbance of specific vibrational modes (e). Using computational methods, it is possible to create a comprehensive description of the tissue cell types (f) in which recognition is achieved without manual intervention.

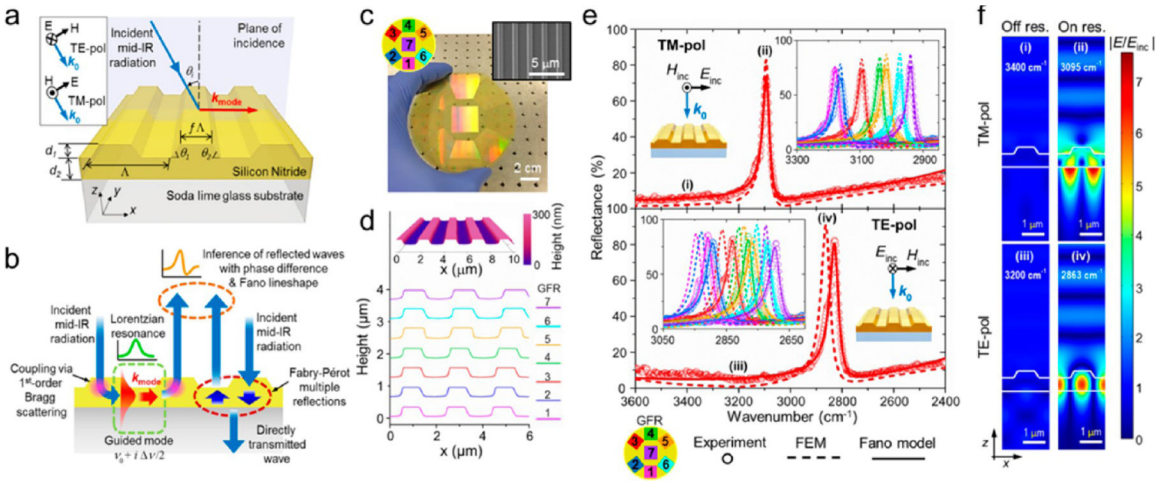

Figure 2.

Large-area mid-IR GFRs with narrow bandwidth and high contrast ratio (CR). (a) Schematic diagram defining the orientation and polarization of incident light and the structural parameters of the GFR. TE, transverse electric. TM, transverse magnetic. (b) Incident mid-IR radiation gets reflected via two channels presented in the structure, Lorentzian narrow-line width guided resonance and broadband Fabry-Perot́ reflection. (c) Optical image of a set of large-area GFRs built on a 4-in. soda lime glass substrate. Top right inset: SEM image of a fabricated structure. (d) AFM cross-sectional profiles, vertically offset for clarity. The 3-D AFM topography image of the structure 7 (GFR-7) is shown in the top inset. (e) Measured and FEM-computed far-field reflectance spectra of a representative device (GFR-3) when a TM-polarized (top) or TE-polarized (bottom) light is normally incident, along with the zoomed-in spectra in the vicinity of the resonances of all GFRs as shown in the inset. Each experimental spectrum is also fitted with the Fano interference model. (f) FEM-computed electric field amplitude ($|E/E_{inc}|$) distributions in a unit cell of the GFR-3 at the indicated spectral locations in (e).

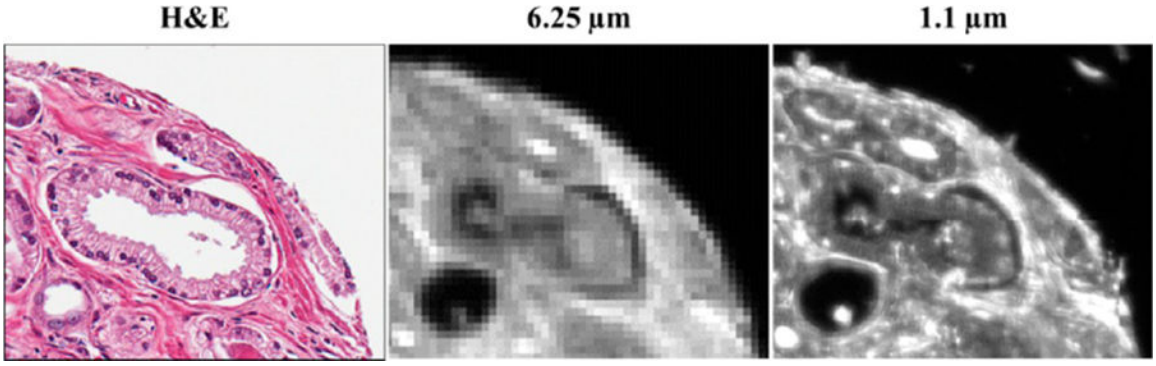

Figure 3.

Comparison of high-definition and standard IR imaging with optical microscopy of tissue. A section of a prostate tissue section stained with H&E and imaged using FT-IR with normal magnification and in high definition (intensity at 3300 cm^{-1} is shown).

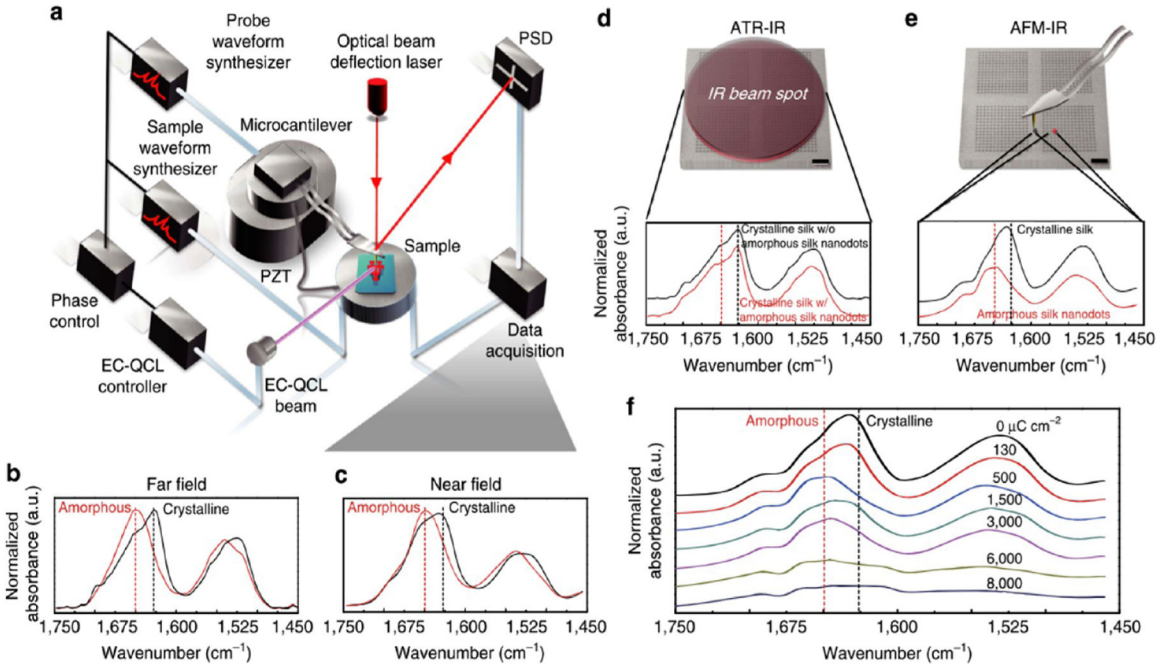

Figure 4.

Quantitative evaluation of conformational transitions in silk proteins using near-field IR nanospectroscopy. (a) Schematics of IR nanospectroscopy using AFM−IR: pulses of IR radiation emitted by an IR QCL (output range: 1460−1780 cm^{-1}; swept by a step size: 1 cm^{-1}) were used to illuminate the sample, causing a rapid thermal expansion of silk nanostructures due to local absorption enhancement at various stages picked by the AFM tip, corresponding to the absorption spectroscopic signatures. (b, c) The AFM−IR spectra on amorphous and crystalline silk thin films are consistent with the conventional bulk FT-IR spectra. (d, e) Spectra of a crystalline silk thin film with embedded amorphous silk nanopatterns of ~30 nm fabricated using EBL, characterized by attenuated total reflection IR (ATR-IR) and AFM−IR, respectively. AFM−IR offers a considerable advancement (~1000× improvement spatially) in distinguishing nanoscale structural heterogeneity. (f) AFM−IR spectra of electron-induced structural transitions in silk proteins. PSD, position sensing detectors; PZT, lead zirconate titanate ($Pb[Zr_xTi_{1-x}]O3$); EC-QCL, external cavity quantum cascade laser. Reprinted by permission from Macmillan Publishers Ltd.: NATURE, Qin, N.; Zhang, S.; Jiang, J.; Corder, S. G.; Qian, Z.; Zhou, Z.; Lee, W.; Liu, K.; Wang, X.; Li, X.; Shi, Z.; Mao, Y.; Bechtel, H. A.; Martin, M. C.; Xia, X.; Marelli, B.; Kaplan, D. L.; Omenetto, F. G.; Liu, M.; Tao, T. H. *Nat. Commun.* **2016**, *7*, 13079 (ref 123). Copyright 2016.

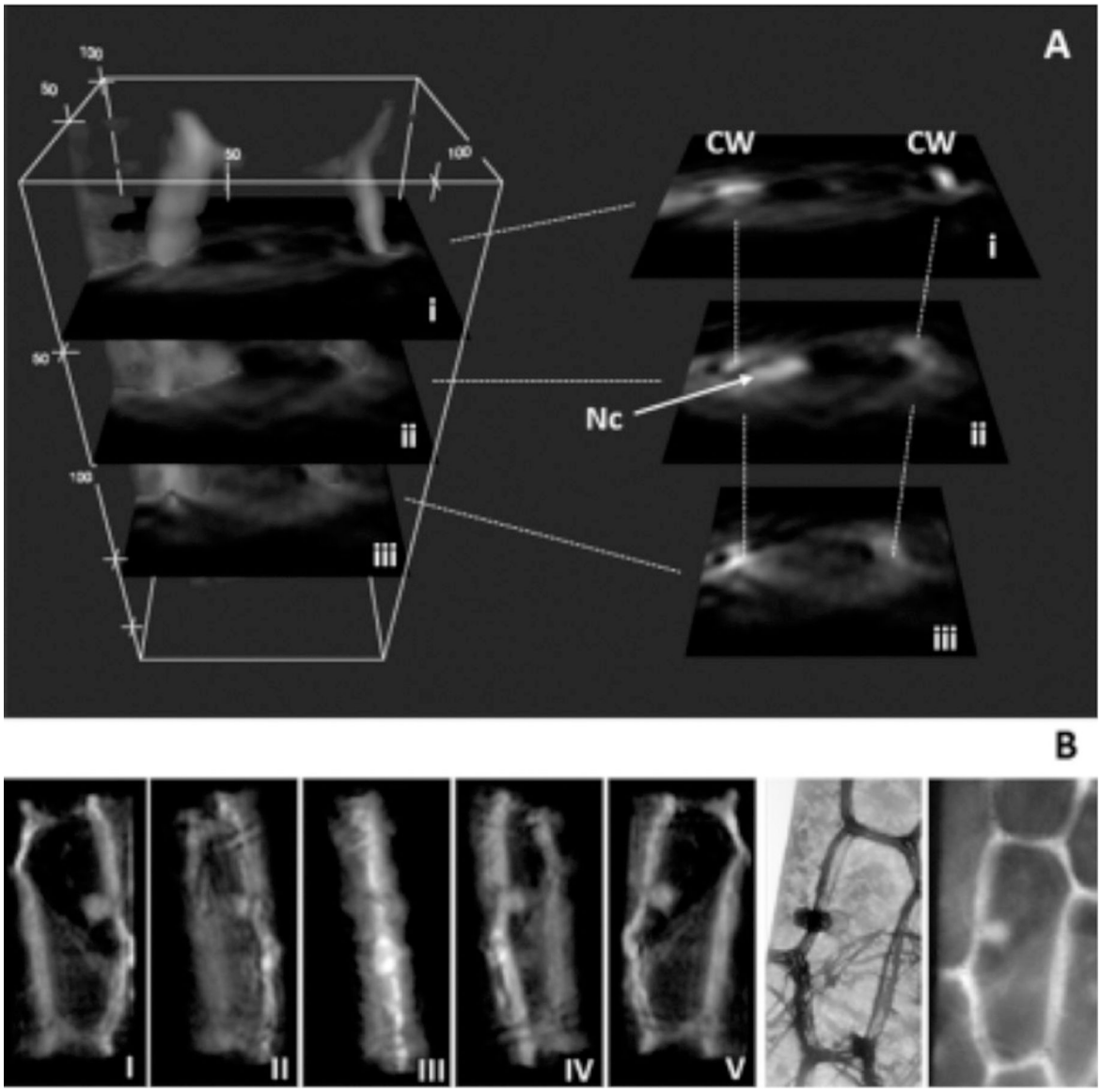

Figure 5.

3D computed tomography reconstruction of the cellular distribution of the A1 stretching frequency of compound **1.** (A) Reconstructed volume rendering with digital slicing at selected locations. Stacked slices on the right correspond to volume positions on the left. CW = cell wall; Nc = nucleus. Vertical dotted lines connect locations of the highest A1 area intensity on the CW. (B) Volume rendering visualized as a function of rotation about the vertical axis. From left to right: 45° rotation steps starting at 0° (I) to 180° (V). The rotation series is accompanied by a laser scanning transmission image at 488 nm illustrating a projection of the detailed structure of the cell and one of the 2D IR maps of the A1 band used for reconstruction. Reproduced from Three-Dimensional Mid-Infrared Tomographic Imaging of Endogenous and Exogenous Molecules in a Single Intact Cell with Subcellular Resolution, Quaroni, L.; Obst, M.; Nowak, M.; Zobi, F. *Angew. Chemie Int. Ed.* **2015**, *54* (1), 318−322 (ref 140). Copyright 2015 Wiley.

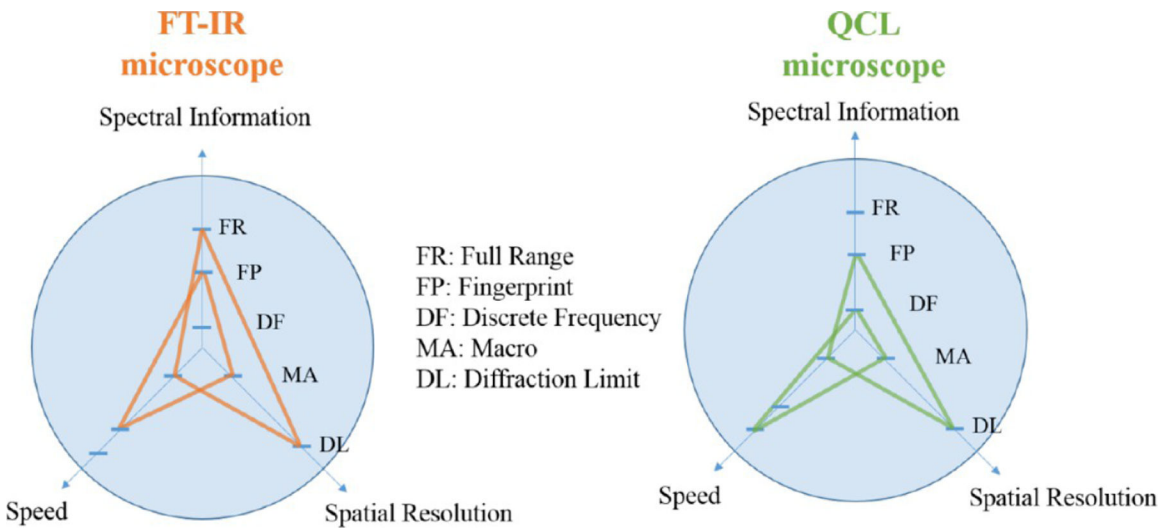

Figure 6.

A comparison between current FT-IR and DFIR microscopes' capabilities in terms of dependencies of spectral content, spatial resolution, and the resulting acquisition speed. While spectral bandwidth (and information content) of FT-IR imaging is large, speed of data acquisition is slow. By compressing the spectral axis, DF methods can match spatial detail but considerably speed up data acquisition. Multiaxes views of the type shown can be used to compare instruments and experiments rapidly.

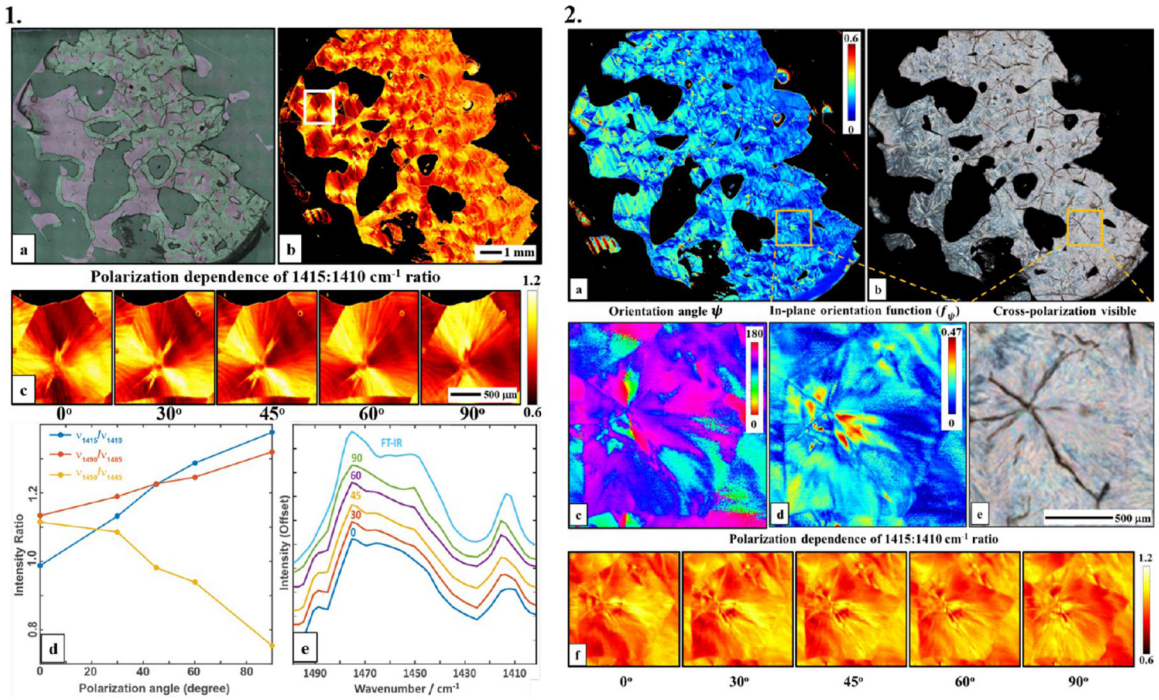

Figure 7.

[Left panel] (a) Visual image of a PEG polymer film. (b) Intensity map of 1415:1410 cm^{-1} ratio at 0° polarization visualizing the spherulite crystal structure. (c) A zoom of area in the white box in 1b, taken with 5 polarizations: 0, 30, 45, 60, and 90, respectively. (d) Polarization dependence of selected bands ratios. (e) Average spectra in the 1400−1500 cm^{-1} range of a selected region (white circle) taken with different polarizations and compared to a FT-IR spectrum of the same sample. The spectra have been offset for clarity. [Right panel] (a) In-plane orientation function calculated using CH_2 wagging vibration at 1410 cm^{-1} wavenumber. (b) A visible cross-polarization image. (c) Azimuthal angle distribution of molecular chains in the zoom from (a). (d) A zoom in of the in-plane orientation function of (a) showing the borders of the spherulite. (e) A zoom in on the same area in the cross-polarization visible image. (f) 1415:1410 cm^{-1} ratio distribution with different polarizations of the same area. Reproduced from Wrobel, T. P.; Mukherjee, P.; Bhargava, R. *Analyst* **2017**, *142* (1), 75−79 (ref 31) with permission from the Royal Society of Chemistry.

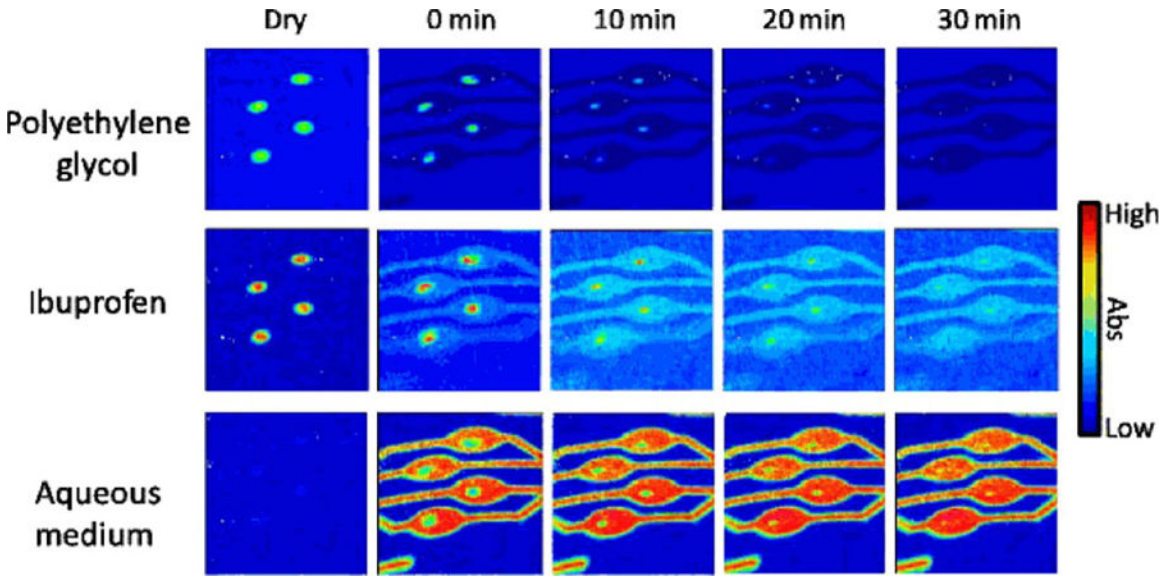

Figure 8.

ATR-FT-IR spectroscopic images showing the simultaneous dissolution of four ibuprofen/PEG (1:3 weight ratio) formulations in neutral solution. The spatial distribution of PEG (top row), ibuprofen (middle row), and the aqueous solution (bottom row) have been presented. The dimensions of the images are ~11.5 × 8 mm^2.[161] Reproduced from Ewing, A. V; Clarke, G. S.; Kazarian, S. G. *Biomicrofluidics* **2016**, *10* (2), 24125, with the permission of AIP Publishing.

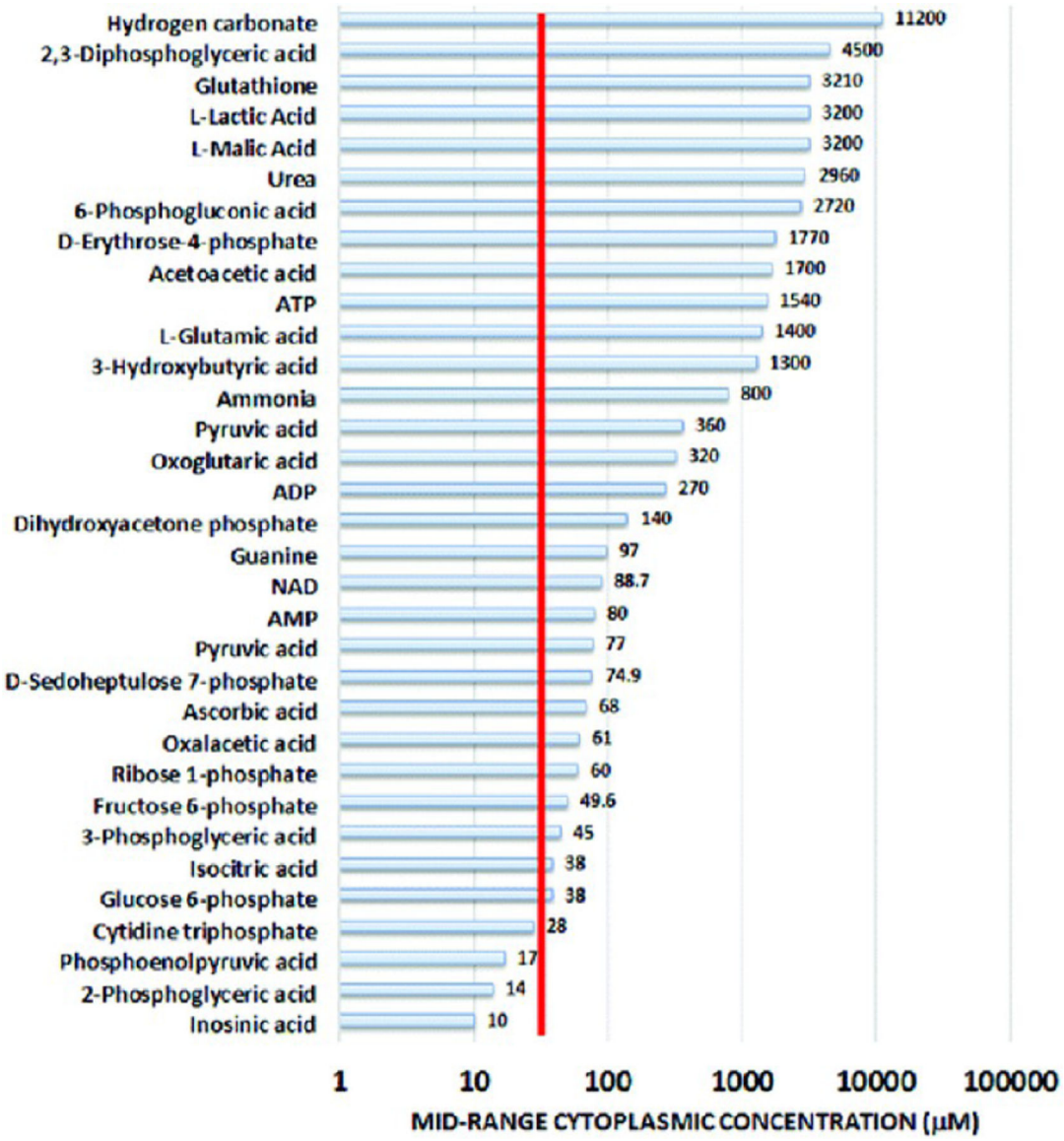

Figure 9.

Reported cytoplasmic concentrations of human metabolites from the Human Metabolome Database (HMDB). The red line shows a recently reported limit for the detectability of a small molecule in an FT-IR measurement. Reproduced from Chan, K. L. A.; Fale, P. L. V. *Anal. Chem.* **2014**, *86*, 11673−11679 (ref 238). Copyright 2014 American Chemical Society.

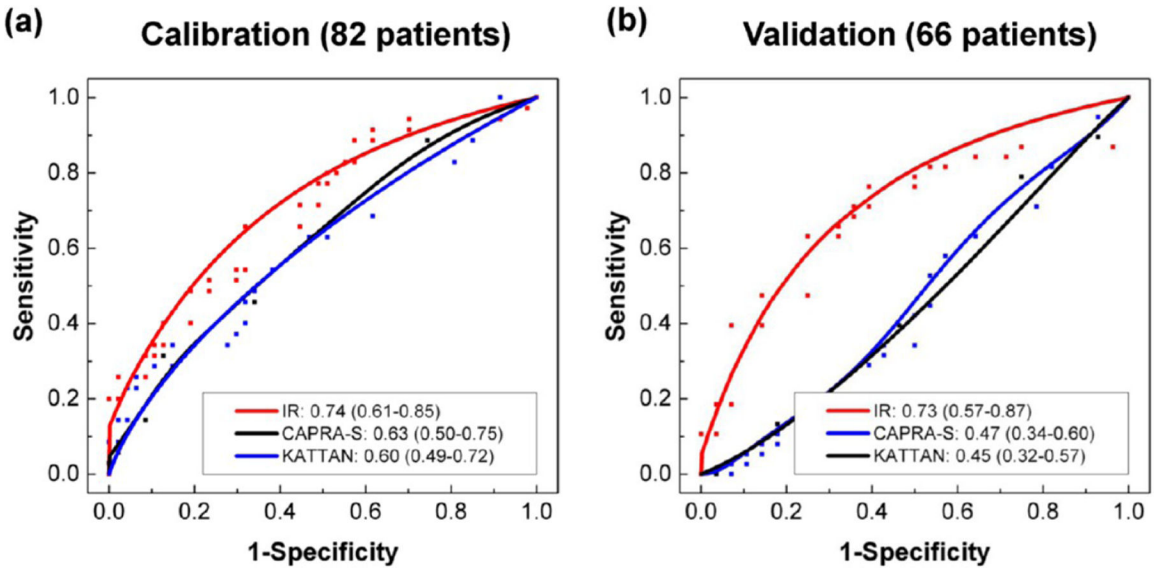

Figure 10.

Performance of outcome prediction. Outcome prediction of three models, CAPRA-S (black), KATTAN nomogram (blue), and IR (red), on (a) the calibration data set and (b) the validation data set. AUCs and 95% confidence intervals in parentheses are shown on the plots. Lines represent the smoothed ROC curves, and rectangular dots denote the empirical sensitivity and 1-specificity points. Reprinted by permission from Macmillan Publishers Ltd.: Scientific reports (Kwak, J. T.; Kajdacsy-Balla, A.; Macias, V.; Walsh, M.; Sinha, S.; Bhargava, R. *Sci. Rep.* **2015**, *5*, 8758), copyright 2015 (ref 240).